

Rubidium  $5S_{1/2} \rightarrow 7S_{1/2}$  two-photon transition

Ming-Sheng Ko  
National Tsing Hua University

July 28, 2004

## Abstract

# Rubidium $5S_{1/2} \rightarrow 7S_{1/2}$ two-photon transition

Master's dissertation

Ming-Sheng Ko

National Tsing Hua University, Taiwan 2004

Rubidium  $5S_{1/2} \rightarrow 7S_{1/2}$  two-photon transition has been observed using a 760 nm external cavity diode laser and a vapor cell. With 10 mW laser power, the SNR and linewidth of the transition is 280 and 3 MHz, respectively. The ECDL is stabilized on the transition to an uncertainty of 7 kHz ( $2 \times 10^{-11}$ ) using FM spectroscopy.

Absolute frequencies of all hyperfine components in this transition have been measured to an uncertainty of 20 kHz using optical femtosecond comb. Different systematic effects are tabled. The uncertainty of hyperfine constant in rubidium  $7S_{1/2}$  state is improved by a factor of four, comparing with previous best result. And for the first time, isotope shift of this transition is measured to be 131.567(73) MHz.

By frequency doubling technique, a 1520 nm ECDL is stabilized on the two-photon transition. This provides a frequency standard in telecommunication band (1460-1530 nm, S-band).

# Contents

<b>1</b>	<b>Introduction</b>	<b>1</b>
1.1	Optical frequency standard based on High resolution spectroscopy . .	1
1.1.1	Doppler-free spectroscopy . . . . .	2
1.1.2	Importance of frequency standards . . . . .	4
1.2	Two-photon transition . . . . .	6
1.2.1	Lineshape of two-photon transitions . . . . .	7
1.2.2	Transition probability . . . . .	7
1.2.3	Light shifts (AC Stark effect) . . . . .	9
1.2.4	Unique potential using two-photon transition . . . . .	10
1.2.5	Limitation of two-photon transition . . . . .	11
1.3	Optical femtosecond comb based on Mode-locked Ti:sapphire laser . .	12
1.3.1	Measurement of optical frequency using femtosecond comb . .	12
1.4	Layout of this thesis . . . . .	13
<b>2</b>	<b>Rubidium <math>5S_{1/2} \rightarrow 7S_{1/2}</math> two-photon transition</b>	<b>15</b>
2.1	Comparison between $5S \rightarrow 7S$ and $5S \rightarrow 5D$ two-photon transitions . . .	15
2.2	Energy level diagram . . . . .	16
2.3	Using 760 nm ECDL as light source . . . . .	17
2.3.1	Laser system . . . . .	19
2.3.2	Anamorphic prism pair . . . . .	19
2.3.3	Cell and heating system . . . . .	20
2.3.4	Detecting system . . . . .	20
2.3.5	light shielding system . . . . .	21

---

2.4	Results . . . . .	21
2.5	Reduction of laser linewidth . . . . .	22
2.6	Using light source doubled from 1520 nm ECDL by PPLN waveguide	22
<b>3</b>	<b>Absolute frequency measurement using optical femtosecond comb based on mode-locked Ti:sapphire laser</b>	<b>32</b>
3.1	Femtosecond comb system . . . . .	32
3.2	Method one: Stabilize the laser on the transition . . . . .	34
3.3	Method two: Offset-lock the laser on the comb . . . . .	36
3.4	Results . . . . .	37
3.4.1	Absolute frequencies of rubidium $5S_{1/2} \rightarrow 7S_{1/2}$ two-photon transitions . . . . .	37
3.4.2	Reproducibility of the measurements . . . . .	37
3.4.3	Systematic effects . . . . .	38
3.4.4	Hyperfine Constant of Rubidium 7S state . . . . .	42
3.4.5	Isotope shift . . . . .	43
<b>4</b>	<b>Conclusion</b>	<b>44</b>

# List of Figures

1.1	Two-photon diagram. . . . .	7
1.2	Energy level diagram of two-photon transition. Where $\hbar\Delta\omega$ is energy detuning, $\omega_0$ is the transition angular frequency, $E_r$ is a real state between ground state $E_g$ and excited state $E_e$ . . . . .	8
1.3	The Doppler background comes from absorbing two photons travelling in the same direction. . . . .	9
1.4	Lineshape simulation of two-photon transitions. . . . .	10
1.5	Frequency spectrum of comb lines and the unknown laser frequency. The frequency difference between the laser and nearby comb line is beat frequency. . . . .	13
2.1	Rubidium pressure versus temperature. . . . .	17
2.2	Partial energy level diagram of rubidium. (not scaled) . . . . .	20
2.3	Experimental setup using 760 nm ECDL. . . . .	24
2.4	Anamorphic prism pair. . . . .	25
2.5	Heating cell design. . . . .	25
2.6	Fluorescence collection and detection system design. . . . .	26
2.7	Spectrum of 5S-7S two-photon transition. The frequency coordinate is determined by fringe marker of the reference cavity. . . . .	27

2.8	Lineshape of the $^{85}\text{Rb}:5\text{S}_{1/2}(\text{F}=3) \rightarrow ^{85}\text{Rb}:7\text{S}_{1/2}(\text{F}=3)$ transition at $110^\circ\text{C}$ . The signal is fitted to a Lorentzian lineshape with $\text{FWHM}=2.8$ MHz and $\text{SNR}=280$ . The inset shows the measured linewidth versus the temperature of vapor cell. Each point is the average of 10 measurements. . . . .	27
2.9	The zero-crossing lineshape generated by frequency-modulation spectroscopy. The SNR and linewidth (peak-to-peak) are 100 and 5.1 MHz, respectively. . . . .	28
2.10	Allan deviation derived from the residual error signal while the laser was locked on the $^{85}\text{Rb}:\text{F}=3-3$ two-photon transition. Inset shows the residual error signal. . . . .	28
2.11	Differential detector. . . . .	29
2.12	The ECDL is preliminary stabilized on the side fringe of a confocal tunable cavity. The linewidth of the diode laser after stabilization is 0.8 MHz. . . . .	29
2.13	Experimental setup. The light source was frequency doubled from 1520 nm ECDL. . . . .	30
2.14	Derivative-like lineshape using frequency modulation technique. The signal-to-noise ratio is 30. The following noise shows the 1520 nm ECDL locked on $^{85}\text{Rb}:\text{F}=3-3$ two-photon transition through frequency doubling. . . . .	31
2.15	Allan deviation derived from the residual error signal while the 1520 nm ECDL was locked on $^{85}\text{Rb}:\text{F}=3-3$ transition through frequency doubling. . . . .	31
3.1	The femtosecond comb system setup by the Center for Measurement Standards. DMs: dichroic mirrors; APDs: avalanche photodiodes; SHG: second-harmonic generation; AOM: acoustic-optic modulator; PZT: piezoelectric transducer. . . . .	33
3.2	Absolute frequency measurement setup. The 760 nm laser is stabilized on the two-photon transition while the comb is self-referenced. . . . .	34

---

3.3	The beat signal between comb lines at 760 nm and the rubidium-stabilized laser. The resolution bandwidth is 100 kHz. . . . .	35
3.4	Beat frequency from counting the beat note. Gate time of the counter is 1 second. Typically, the standard deviation of the beat frequency is 15 kHz. . . . .	36
3.5	Allan deviation of the beat frequency between self-referenced comb and rubidium-stabilized laser. . . . .	37
3.6	Absolute frequency measurement setup. The 760 nm laser is offset-locked on the comb line by the frequency of synthesizer. . . . .	38
3.7	The signal of the transition using offset-lock scheme. The 760 nm laser is offset-locked on the comb line by the frequency of synthesizer. Frequency of the synthesizer is scanned using GPIB interface. Therefore, the laser frequency is scanned across the transition. The scanning range of synthesizer is 20 MHz in this measurement. Each scan is taken within 90 seconds. . . . .	39
3.8	The measured frequency of the Rb <sup>87</sup> F=1-1 two-photon transition. The 760 nm laser power is 7 mW and the temperature of rubidium cell is 130 <sup>o</sup> C. Data 1 ~ 4 are taken within 40 days using method 1 (stabilize the laser on the transition). Data 5 is taken using method 2 (offset-lock the laser on the comb line). Results of the two methods agree to each other. . . . .	40
3.9	Frequency shift of the two-photon line center versus the pressure in rubidium cell. The 760 nm laser is stabilized on the Rb <sup>87</sup> F=2-2 two-photon transition. . . . .	41

# List of Tables

1.1	Various frequency standards based on atomic and molecular transitions.	2
1.2	ITU~T grid. S-band: 1460-1530 nm, C-band: 1530-1565 nm, L-band: 1565-1625 nm. . . . .	5
2.1	Comparison between rubidium $5S \rightarrow 7S$ and $5S \rightarrow 5D$ two-photon transitions . . . . .	16
2.2	Rb pressure versus temperature. . . . .	18
2.3	Decay channels of rubidium $7S$ state . . . . .	19
3.1	The measured absolute frequencies of Rb $5S_{1/2} \rightarrow 7S_{1/2}$ two-photon transitions. The 760 nm laser power is 7 mW and the temperature of the cell is $130^\circ\text{C}$ . . . . .	38
3.2	Summary. . . . .	42
3.3	The absolute frequencies of rubidium $5S_{1/2} \rightarrow 7S_{1/2}$ two-photon transition after correction of different systematic effects. . . . .	42
3.4	The hyperfine constant $A$ of rubidium $7S_{1/2}$ state in MHz. . . . .	43

# Chapter 1

## Introduction

### 1.1 Optical frequency standard based on High resolution spectroscopy

Measurements of optical frequency have played an important role in testing the fundamental physics and have motivated the development of quantum mechanics [1]. Furthermore, studies of hyperfine structure splitting and isotope shifts have contributed to our understanding of the nucleus [2]. Since the atomic and molecular energy levels are constant physics quantities, they can provide universal and reproducible frequency standards.

Various frequency standards are listed in Table. 1.1. The primary frequency standard is based on the ground state hyperfine transition (9192631770 Hz) of the Cesium [3]. All the secondary frequency standards are based on the primary frequency standard with frequency chain [4].

The limitation of accurate measurements in the optical frequency of a gas sample is mainly due to the random motion of the gas particles. The random motion of the particles toward or away from the exciting light source will produce a frequency shift proportional to the velocity of the atom (Doppler effect). Thus the spectrum appears to be a broad Gaussian lineshape, rather than the narrow Lorentzian lineshape caused by the finite lifetime of the upper level. In high resolution spectroscopy, many

techniques have been devised to overcome the limitations of Doppler broadening.

Frequency standard	Atom/molecule	Frequency/Wavelength	Method
Primary	Cesium	9192631770Hz [3]	Atomic beam / Fountain
Secondary	Iodine	532-nm [5]	Saturation spectroscopy
Secondary	CH <sub>4</sub>	3.39- $\mu$ m [6]	Saturation spectroscopy
Secondary	C <sub>2</sub> H <sub>2</sub>	1542-nm [7]	Saturation spectroscopy
Secondary	Rb	778-nm [8]	Two-photon spectroscopy
Secondary	Rb	760-nm [this work]	Two-photon spectroscopy

Table 1.1: Various frequency standards based on atomic and molecular transitions.

### 1.1.1 Doppler-free spectroscopy

#### Atomic beam spectroscopy

Atomic beam technique reduces the Doppler broadening effect by reducing the component of velocity in the direction of the observer, and also provides a collision-free environment. This technique allows measurements at any frequency but the disadvantage of this technique is the low number density, which interacts with light source, and low signal strength [9].

#### Laser-cooling spectroscopy

The magneto-optical trap (MOT) is now used to provide samples of laser-cooled atoms for a range of experiments. It is possible to prepare atomic samples with ensemble temperatures below  $20\mu$ K and densities greater than  $10^{11}$  cm<sup>-3</sup> by using a relatively simple setup [10].

The velocity of atoms in the MOT is greatly reduced to a few cm/sec. The Doppler, collisional and transit time broadening effects are greatly reduced; dense and isotropically pure samples can be produced. This provides an excellent environment for high resolution spectroscopy. The disadvantage of MOT for spectroscopy is that it is difficult to trap two different isotopes at the same time. Therefore, the isotope shift can not be directly measured in such an environment. The trapping magnetic field is also a disturbance for long period measurement.

### Saturation spectroscopy

The technique of Doppler-free saturated absorption spectroscopy was developed by the research group of Arthur L. Schawlow, who was one of the recipients of the 1981 Nobel Prize in physics for this work [11].

The experimental apparatus includes two counterpropagating beams, one is a strong pump beam and the other is a weak probe beam. The two counterpropagating laser beams produce a Doppler-free saturation dip (Lamb dip) in the center of a Doppler-broadened line. When the laser frequency is tuned off line center, one beam interacts with  $+\vec{k}\cdot\vec{V}$  atoms, while the beam propagating in the opposite direction interacts with  $-\vec{k}\cdot\vec{V}$  atoms. At the center of the Doppler line both laser beams interact with the same velocity group ( $\vec{k}\cdot\vec{V}=0$ ). When the intensity of the pump beam is high enough to saturate the transition, the atoms will be more transparency for the probe beam. Therefore, the absorption lineshape of the probe beam appears as a much narrower Lamb dip.

The limitation of the saturated absorption spectroscopy is that it needs enough power to saturate the transition. In some weak transitions, the saturation power could be as high as 100 mW. This can not be achieved in many wavelength regions that lack of powerful lasers.

### Two-photon spectroscopy

In two-photon transitions, the Doppler broadening is eliminated by using two counterpropagating beams. In the atomic frame of reference, the two laser beams appear at frequencies of  $\omega_0(1-\frac{\vec{k}\cdot\vec{V}}{c})$  and  $\omega_0(1+\frac{\vec{k}\cdot\vec{V}}{c})$ , where  $\omega_0$  is the frequency halfway between the two-photon levels. The velocity dependent Doppler shift is cancelled, indicating that, at resonance, all the atoms, irrespective of their velocities, can absorb the two photons. Theoretically, the width of this resonance is natural linewidth. Due to the absorption of two photons travelling in the same direction, the lineshape will have a Doppler background with a small intensity and broad width. In optical frequency region, the Doppler background is approximately 1/1000 of the two-photon resonance in amplitude. The limitation of two-photon transitions is that it can be used only in

E1 forbidden transitions ( $S \rightarrow S$ ,  $S \rightarrow D$ , or  $P \rightarrow P$ ).

### 1.1.2 Importance of frequency standards

#### Frequency standard and metrology

Frequency is the most precise physical quantity that has been measured, and the definition of time is directly related to the definition of frequency. One of the most important applications of atomic frequency standards is to provide the definition of time. Currently, the primary clock is the Cesium atomic clock. The radio frequency (9192631770 Hz) is locked to the ground state hyperfine transition of Cesium. The time interval that the radio frequency oscillates 9192631770 times is defined to be 1 second. From the definition of time scale and the defined velocity of light, the unit length is then derived [12].

#### Frequency standard and fundamental constant

High-precision spectroscopy is useful in testing fundamental principles. Lamb shift, Rydberg constant can be measured in the spectroscopy of simple atoms [13]. Furthermore, studies of hyperfine structure splitting and isotope shifts have contributed to our understanding of the nucleus.

#### Frequency standard and industrial applications

In order to increase the transmission bandwidth in telecommunication, Wavelength Division Multiplexing (WDM) was introduced in 1995. Instead of increasing modulation rate, the WDM system increases the bandwidth by increasing carriers in different wavelengths. The ITU (International Telecommunication Union) has proposed a set of closely-spaced wavelengths in the 1550 nm window. These different wavelengths or channels, are spaced 100 GHz apart, which is approximately 0.8 nm. This set of channels is commonly known as the ITU-T grid, and is specified in frequency. The channel wavelength and frequency allocation is listed in Table. 1.2.

In telecommunication, the Acetylene ( $C_2H_2$ ) and Hydrogen Cyanide (HCN) are good

candidates for optical frequency standards due to their broad absorption lines in this wavelength region.  $C_2H_2$  provides a large number of reference transitions in the 1512-1542 nm and HCN creating absorption lines in the 1528-1563 nm. To perform  $C_2H_2$  Doppler-free saturation spectroscopy, due to the weak oscillation strength, needs a power of  $>100$  mW [7]. HCN is a hypertoxic gas; it is dangerous to handle the HCN gas cell. The Doppler broadened absorption lines of these absorbers are 2-3 GHz wide. They have been in commercial use to calibrate the optical spectrum analyzer (OSA) in GHz accuracy.

Channel Code	Freq(THz)	$\lambda$ (nm)	Channel Code	Freq(THz)	$\lambda$ (nm)
25	192.5	1557.36	51	195.1	1536.61
26	192.6	1556.55	52	195.2	1535.82
27	192.7	1555.75	53	195.3	1535.04
28	192.8	1554.94	54	195.4	1534.25
29	192.9	1554.13	55	195.5	1533.47
30	193.0	1553.33	56	195.6	1532.68
31	193.1	1552.52	57	195.7	1531.90
32	193.2	1551.72	58	195.8	1531.12
33	193.3	1550.92	59	195.9	1530.33
34	193.4	1550.12	60	196.0	1529.55
35	193.5	1549.32	61	196.1	1528.77
36	193.6	1548.51	62	196.2	1527.99
37	193.7	1547.72	63	196.3	1527.22
38	193.8	1546.92	64	196.4	1526.44
39	193.9	1546.12	65	196.5	1525.66
40	194.0	1545.32	66	196.6	1524.89
41	194.1	1544.53	67	196.7	1524.11
42	194.2	1543.73	68	196.8	1523.34
43	194.3	1542.94	69	196.9	1522.56
44	194.4	1542.14	70	197.0	1521.79
45	194.5	1541.35	71	197.1	1521.02
46	194.6	1540.56	72	197.2	1520.25
47	194.7	1539.77	73	197.3	1519.48
48	194.8	1538.98	74	197.4	1518.71
49	194.9	1538.19	75	197.5	1517.94
50	195.0	1537.40	76	197.6	1517.17

Table 1.2: ITU~T grid. S-band: 1460-1530 nm, C-band: 1530-1565 nm, L-band: 1565-1625 nm.

## 1.2 Two-photon transition

Unlike one photon resonance, two-photon transition is that the atom is excited from ground state to excited state by absorbing two counterpropagating photons (see Fig. 1.1). Energy-level diagram of two-photon transition is shown in Fig. 1.2. Assuming that a two-photon transition can occur between the levels  $E_g$  and  $E_e$  of an atom in counterpropagating waves of angular frequency  $\omega_0$ .

$$E_e - E_g = \hbar(\omega_0 + \vec{k} \cdot \vec{V}) + \hbar(\omega_0 - \vec{k} \cdot \vec{V}) = 2\hbar\omega_0. \quad (1.1)$$

If  $\vec{V}$  is the velocity of the atom,  $+\vec{k}$  is the wavevector of forward propagating beam and  $-\vec{k}$  is the wavevector of reverse propagating beam. The first-order Doppler shift of the forward beam and backward beam is  $\vec{k} \cdot \vec{V}$  and  $-\vec{k} \cdot \vec{V}$ , respectively. Thus the first-order Doppler shift cancel out and the energy of the two photons seen by an atom is  $2\hbar\omega$  irrespective of its velocity. Only when  $\omega = \omega_0$  will the atoms at the ground state be excited to the excited state by two-photon absorption. Therefore, the linewidth of the two-photon transition is limited only by the lifetime of the upper level (natural linewidth) and the lineshape will be Lorentzian.

$$\hbar(\omega + \vec{k} \cdot \vec{V}) + \hbar(\omega - \vec{k} \cdot \vec{V}) = 2\hbar\omega. \quad (1.2)$$

Instead of stepwise excitation (two successive one-photon excitation), the atom at the ground state is directly excited to the excited state by two-photon absorption. The energy detuning is the most important parameter in calculating the two-photon transition rate. There is no real transition from the ground state to the virtual intermediate state. The transition probability comes from the Lorentzian tail of the real transitions nearby ( $E_g \rightarrow E_r$  and  $E_r \rightarrow E_e$ ). Consequently, the smaller the energy detuning, the stronger the two-photon transition is.

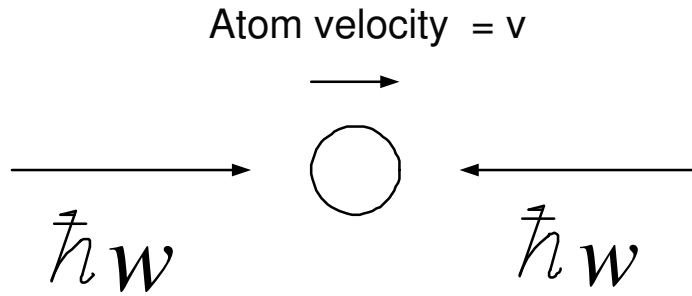


Figure 1.1: Two-photon diagram.

### 1.2.1 Lineshape of two-photon transitions

Aside from absorbing two photons from the two counterpropagating beams, the atoms have the possibility to absorb two photons traveling in the same direction (see fig. 1.3). Doppler shift of the two photons travelling in the same direction does not cancel out, and this results in a Doppler background. The two-photon lineshape appears as the superposition of one broadened Doppler background (Gaussian) and a much narrower Lorentzian profile (see fig. 1.4).

Intensity (area) of the Doppler background is half of the Lorentzian [14]. Comparing to the Lorentzian curve, the Doppler background is usually too small to be detected due to its broad width.

### 1.2.2 Transition probability

The transition probability of Doppler-free two-photon transition may be calculated using perturbation theory to second order. The probability of exciting an atom from the ground state  $g$  to an excited state  $e$  is equal to [14]

$$p_{ge}^{(2)}(\delta\omega) = \left| \sum_i \frac{\langle e | H_1 | i \rangle \langle i | H_2 | g \rangle + \langle e | H_2 | i \rangle \langle i | H_1 | g \rangle}{\Delta\omega_i} \right|^2 \frac{\Gamma_e}{4\delta\omega^2 + \frac{1}{4}\Gamma_e^2} \quad (1.3)$$

The notation used is as following:

$\Gamma_e$  is the natural linewidth of the excited state (inverse of the lifetime).

$\delta\omega = \omega - \omega_0$  is the difference between the laser angular frequency  $\omega$  and the resonance frequency  $\omega_0 = (E_e - E_g)/2\hbar$ .

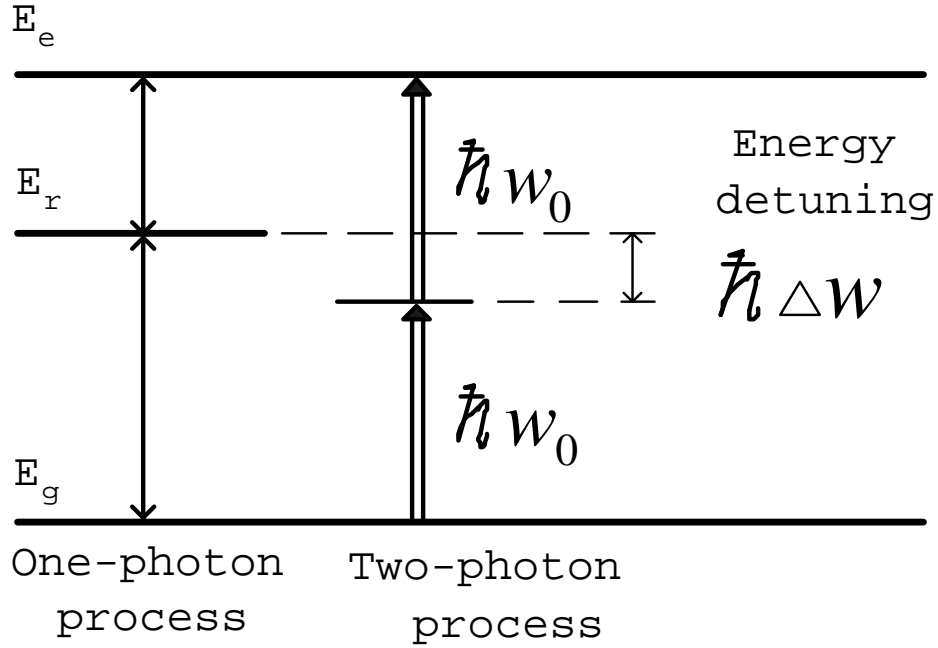


Figure 1.2: Energy level diagram of two-photon transition. Where  $\hbar\Delta\omega$  is energy detuning,  $\omega_0$  is the transition angular frequency,  $E_r$  is a real state between ground state  $E_g$  and excited state  $E_e$ .

$H_1$  and  $H_2$  are the Hamiltonians (divided by  $\hbar$ ) of the atom with the incident and reflected waves (electric dipole interaction).

$\hbar\Delta\omega_i = \hbar\omega_0 - (E_i - E_g)$  is the energy detuning of the one-photon transition for each intermediate state  $i$ . It is assumed that  $\Delta\omega_i$  is much bigger than the Doppler width of the transition  $g \rightarrow i$  to ensure that there is no stepwise excitation.

The term  $\Gamma_e(4\delta\omega^2 + \frac{1}{4}\Gamma_e^2)^{-1}$  is the Lorentzian curve.

If the two oppositely travelling waves are identical (same intensity and same polarization) and at resonance ( $\delta\omega = 0$ ):

$$p_{ge}^{(2)}(res) = \left| \sum_i \frac{\langle e | H_1 | i \rangle \langle i | H_2 | g \rangle}{\Delta\omega_i} \right|^2 \frac{16}{\Gamma_e} \quad (1.4)$$

In short, the probability of the two-photon transition is approximately proportional to the inverse square of the energy detuning.

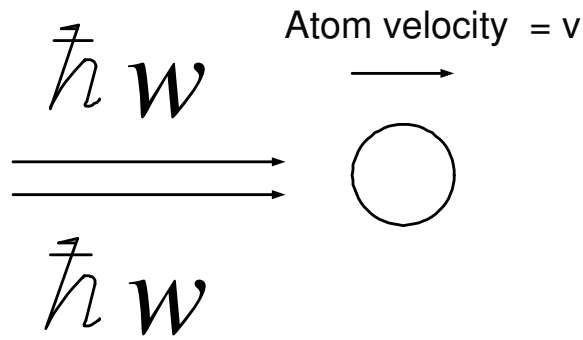


Figure 1.3: The Doppler background comes from absorbing two photons travelling in the same direction.

### 1.2.3 Light shifts (AC Stark effect)

In two-photon transitions, the energy level diagram must have a ground state  $E_g$ , a forbidden upper level  $E_e$  and an allowed real state  $E_r$  near the middle of ground state and upper level. The photon energy of the laser, however, is detuned from  $E_r - E_g$ , and this detuning from real transitions causes light shifts. This effect will result in a systematic factor by shifting the resonance frequency.

The calculation of light shift is as following [14]:

$$\delta\omega_g = 2 \frac{\langle g | H | r \rangle \langle r | H | g \rangle}{\Delta\omega_r} \quad (1.5)$$

$$\delta\omega_e = 2 \frac{\langle e | H | r \rangle \langle r | H | e \rangle}{\Delta\omega_r} \quad (1.6)$$

The factor of 2 corresponds to the two travelling waves (the value of the shift is twice the value in a single travelling wave).

The shift of the two-photon transition is equal to  $(\delta\omega_e - \delta\omega_g)$ . The light shift of the two-photon transition is approximately proportional to the inverse of the energy detuning.

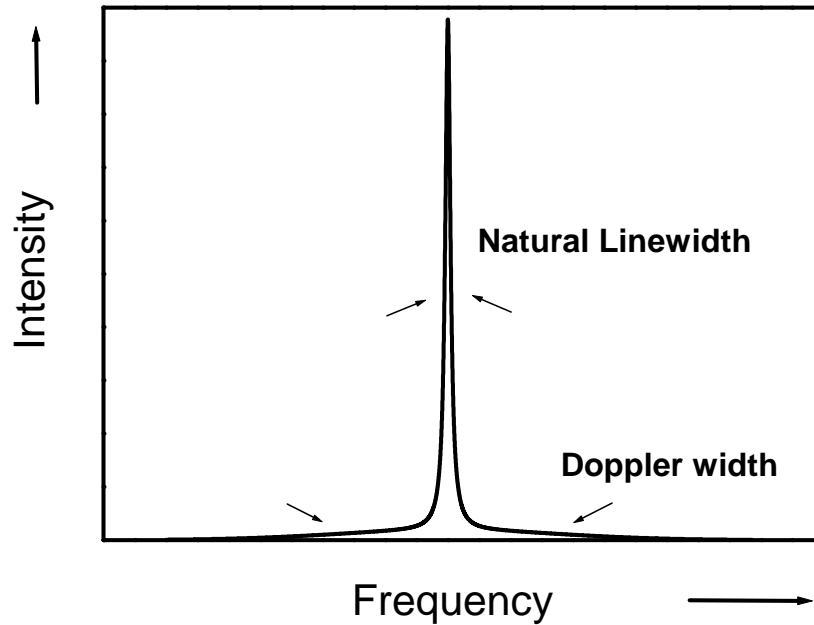


Figure 1.4: Lineshape simulation of two-photon transitions.

## 1.2.4 Unique potential using two-photon transition

### **Zeeman shift free possibility**

One photon transition can not exist between two symmetric states ( $S \rightarrow S$ ) because the selection rule indicates that  $\Delta\ell=0$  transition is forbidden [15]. Therefore, in  $\Delta\ell \neq 0$  transitions, the ground state and excited state have different Landé  $g$  factor due to lack of symmetry. Zeeman shifts of the ground state and the excited state are different under the same magnetic field [16]. Consequently, the transition frequency (difference between the two energy levels) will shift due to magnetic field.

On the contrary, transitions between the  $\Delta\ell=0$  states can exist in two-photon transitions. It is possible to excite an atom from  $S$  state to  $S$  state in two-photon transition [17]. In these transitions, the transition frequencies do not shift with the magnetic field. In other words, these transitions have immunity against magnetic field, and this is a great advantage where earth field is unavoidable.

### A superior long lifetime of the upper level

With  $S \rightarrow S$  possibility, it is possible to excite an atom to a forbidden state which has no allowed decay channels [13]. The lifetime of the upper level becomes superior long and the natural linewidth will be very small.

### 1.2.5 Limitation of two-photon transition

Although, there are several great features of two-photon transition, as described previously, the limitation of this technique can be summarized as following:

1. Two-photon transition is only allowed in E1 forbidden transitions, like  $S \rightarrow S$ ,  $S \rightarrow D$  and  $P \rightarrow P$ .
2. The energy detuning can not be too large in order to have enough transition rates, i.e. there should be a real state near the middle of the ground state and excited state.
3. Light shift, due to the laser frequency detuned from the resonance of the real transition, must be considered. Fortunately, in many cases, these light shifts are generally much smaller than natural linewidth in the case of two-photon transitions [17][18][19].
4. Due to the weak absorption rate of two-photon transition comparing to one-photon resonance, the absorption of exciting laser can not be detected. The signature of the transition must be the fluorescence. Pound-Drever-Hall technique can not be applied to generate the error signal for frequency stabilization. The error signal can be generated by modulating the laser frequency, which will be a challenge in Ti:sapphire laser experiment, but it is not a problem for the semiconductor laser experiment.

## 1.3 Optical femtosecond comb based on Mode-locked Ti:sapphire laser

Optical femtosecond comb is a revolutionary technique in determining the optical absolute frequency. Before the invention of femtosecond comb, the measurement of absolute frequency is complicated. Frequency chain is usually applied in such a measurement [13][19]. Due to the complex and tremendous system of the frequency chain, only few laboratories can afford such a large system and its maintenance. In the chain, the optical frequency is frequency down converted to the radio frequency region by several stages of transfer lasers, and linked to the primary frequency standard, Cesium clock.

Without complexity of chain, the femtosecond comb directly link the optical frequency to the radio frequency region through two parameters, repetition rate  $f_{rep}$  and the offset frequency  $f_o$ .

### 1.3.1 Measurement of optical frequency using femtosecond comb

The optical femtosecond comb generates a frequency ruler in frequency domain by a mode-locked laser. Mode-locked lasers generate ultrashort optical pulses by establishing a fixed phase relationship across a broad spectrum of frequencies (see fig. 1.5).

These comb lines are all longitudinal mode of the laser cavity and are separated by an equal spacing, the free spectral range (F.S.R.) of the cavity. This frequency spacing of these comb lines is equivalent to repetition rate  $f_{rep}$ . Another important parameter of the comb is the offset frequency  $f_o$ . Both  $f_{rep}$  and  $f_o$  are in the radio frequency region. The optical frequency of each comb line is described as [20]:

$$f_n = nf_{rep} + f_o \quad (1.7)$$

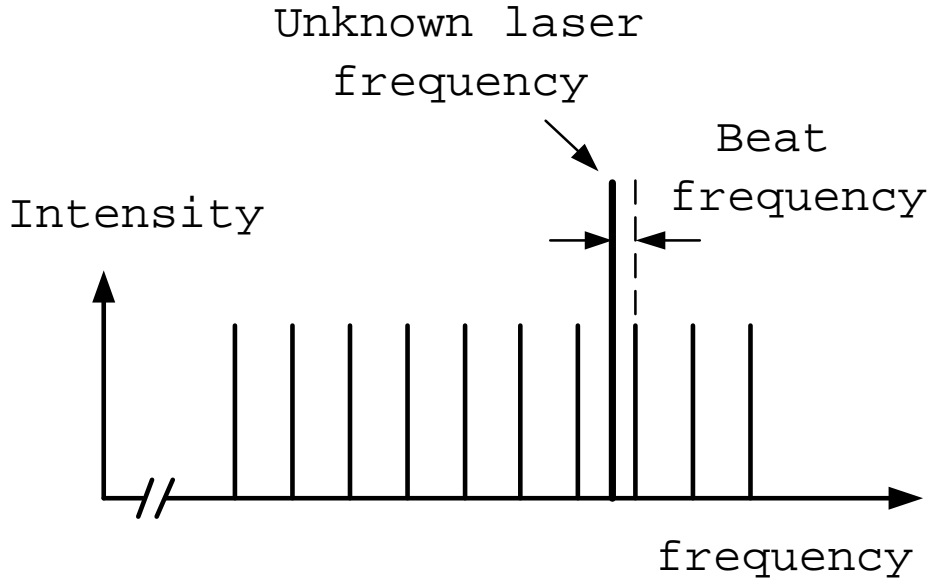


Figure 1.5: Frequency spectrum of comb lines and the unknown laser frequency. The frequency difference between the laser and nearby comb line is beat frequency.

Where  $n$  is a large integer of the order  $10^4$ , and  $f_0$  is the offset frequency.

Therefore, optical frequency is linked to the radio frequency by the generation of femtosecond pulse. If the repetition rate and the offset frequency are both stabilized, absolute frequency of each comb line is known. The absolute frequency of the stabilized laser  $f_\ell$  can be known by the beat frequency  $f_{beat}$  between the comb and the stabilized laser. Thus, the absolute frequency of the stabilized laser can be obtained from

$$f_\ell = n f_{rep} \pm f_0 \pm f_{beat} \quad (1.8)$$

Where  $n$  and the sign of the  $f_0$  and  $f_{beat}$  can be determined by a wavemeter with sub GHz accuracy.

## 1.4 Layout of this thesis

Chapter 2 begins with the study of rubidium  $5S_{1/2} \rightarrow 7S_{1/2}$  two-photon transition. Experimental apparatus and results are presented. Comparison between rubidium  $5S \rightarrow 7S$  and  $5S \rightarrow 5D$  is tabled in this chapter.

Chapter 3 describes the measurement of the absolute frequency in rubidium  $5S_{1/2} \rightarrow 7S_{1/2}$  two-photon transition using optical femtosecond comb. The results include transition frequencies, hyperfine constant and isotope shift. Systematic effects, principally the AC Stark effect and pressure shift, are also discussed.

In conclusion, chapter 4 summarizes the results of this work. Finally, the prospects for future work are proposed.

# Chapter 2

## Rubidium $5S_{1/2} \rightarrow 7S_{1/2}$ two-photon transition

### 2.1 Comparison between $5S \rightarrow 7S$ and $5S \rightarrow 5D$ two-photon transitions

The  $5S \rightarrow 5D$  two-photon transition (778 nm) has been recommended for the realization of meter by CIPM [21]. Its natural linewidth is only 300 kHz [19]. Absolute frequency of this transition has been measured to an uncertainty less than 0.5 kHz [22] [23]. But a serious problem is that the magnetic field causes the transition frequency to shift due to different Landé  $g$  factors of S and D states. On the contrary, the  $5S \rightarrow 7S$  two-photon transition is immune to magnetic field due to the same Landé  $g$  factors of the ground state and excited state. Its natural linewidth is 899.5 kHz.

However, it is not thoroughly Zeeman shift free. In fact, the  $S \rightarrow S$  two-photon transition suppresses only the first-order Zeeman shift, but not the second-order Zeeman shift. In strong magnetic field, it is possible to magnetize the energy levels. It has been measured recently that this kind of magnetization in rubidium can reach tens MHz/ $T^2$  [24]. In 100 Gauss magnetic field, the shift is about 1 kHz. This effect is negligible in laboratory environment where the magnetic field due to the earth field and heating electricity is only a few Gauss.

The detuning of the  $5S \rightarrow 7S$  is 20 nm, which is ten times of that of the  $5S \rightarrow 5D$  two-photon transition (2 nm). Therefore, the transition rate of the  $5S \rightarrow 7S$  is 100 times weaker than that of the  $5S \rightarrow 5D$  two-photon transition. Due to larger detuning, the light shift of the  $5S \rightarrow 7S$  two-photon transition is 1/10 of the  $5S \rightarrow 5D$ 's.

In order to compensate the weak transition rate, the cell was heated to  $120^\circ C$ . Vapor

Transition	$5S \rightarrow 7S$	$5S \rightarrow 5D$
Wavelength	760 nm	778 nm
Intermediate state	$5P_{3/2}$	$5P_{3/2}$
Detuning	20 nm	2 nm
Transition rate	1/100	1
Light shift	1/10	1
Magnetic shielding	No	Yes
Heater	Yes ( $> 120^\circ C$ )	Yes ( $> 90^\circ C$ )
Natural linewidth	899.5 kHz	300 kHz
Laser power	10 mW	1 mW

Table 2.1: Comparison between rubidium  $5S \rightarrow 7S$  and  $5S \rightarrow 5D$  two-photon transitions

pressure of rubidium atom at  $120^\circ C$  is 0.58 mtorr (see Fig. 2.1) corresponding to a number density  $2 \times 10^{21}$  atoms/m<sup>3</sup> [25].

## 2.2 Energy level diagram

The partial energy level diagram of rubidium is shown in Fig. 2.2. There are two naturally occurring isotopes of masses 85 and 87 with nuclear spin 5/2 and 3/2. The naturally occurring abundance of  $^{87}\text{Rb}$  and  $^{85}\text{Rb}$  is 27% and 73%, respectively. The upper level of this transition is  $7S_{1/2}$ , and there are four decay channels of the upper level (see table. 2.3) [26]. In this two-photon transition, the natural linewidth is [27] [28]

$$\frac{(2.64 + 4.4 + 1.409 + 2.854) \text{ MHz}}{2\pi} \times \frac{1}{2} = 899 \text{ kHz} \quad (2.1)$$

The transition selection rule of Zeeman sub-level in S-S two-photon transition is  $\Delta F=0$ . Therefore, there will be four lines in this transition ( $\text{Rb}^{87} F=2-2$ ,  $\text{Rb}^{85} F=3-3$ ,  $\text{Rb}^{85} F=2-2$ ,  $\text{Rb}^{87} F=1-1$ ). The signature of the transition is the 420 nm fluorescence

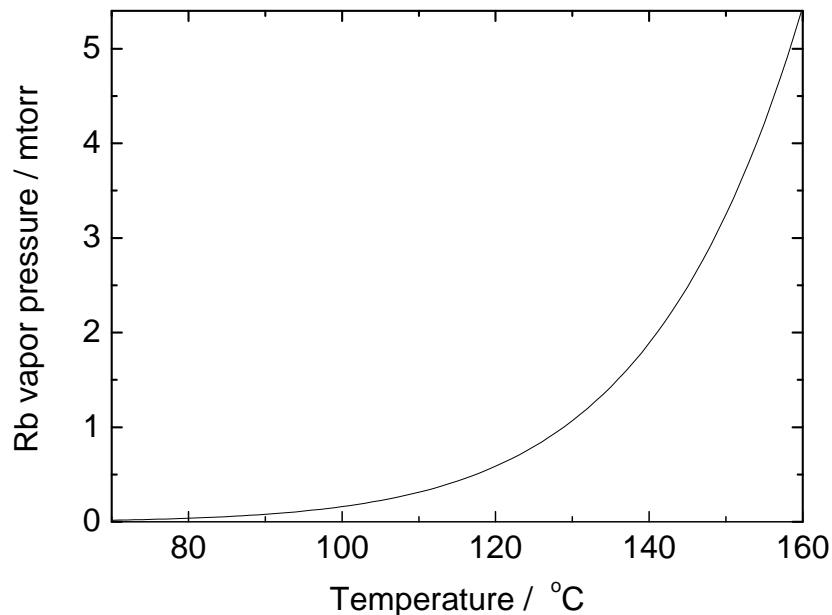


Figure 2.1: Rubidium pressure versus temperature.

from the cascade decays ( $6P \rightarrow 5S$ ). The fluorescence is filtered by a 420 nm band-pass filter to reduce the scattered laser light (760 nm).

### 2.3 Using 760 nm ECDL as light source

The experimental setup is shown in Fig. 2.3. In this experiment, optical feedback is a very severe problem because the laser light is totally retro-reflected. Two stages of isolation were used. The first stage is a double Faraday isolator (OFR IO-5-NIR-LP), which provides approximately 75dB isolation. The second stage is an AOM (INTRACTION) driven by 80MHz rf source. By shifting the frequency of the feedback laser light, one AOM can provide 50dB isolation [29]. The AOM also serves as a fast chopper for modulation of the laser light.

The beam profile of the ECDL output is modified to be Gaussian-like using an anamorphic prism pair. A small portion of light was reflected using a blank plate for laser diagnosis. One of the reflected lights goes through a reference cavity (home-made, F.S.R = 300 MHz) for determine the scanning range of the laser. The other goes to

Temperature( $^{\circ}$ C)	Pressure(mtorr)	Temperature( $^{\circ}$ C)	Pressure(mtorr)
70	0.01715	116	0.45793
72	0.02015	118	0.51886
74	0.02363	120	0.58713
76	0.02767	122	0.66352
78	0.03234	124	0.74891
80	0.03772	126	0.84424
82	0.04393	128	0.95054
84	0.05106	130	1.0689
86	0.05926	132	1.2006
88	0.06865	134	1.347
90	0.0794	136	1.5094
92	0.09169	138	1.6896
94	0.1057	140	1.8891
96	0.12167	142	2.1098
98	0.13983	144	2.3537
100	0.16046	146	2.6231
102	0.18385	148	2.9201
104	0.21035	150	3.2475
106	0.24031	152	3.6078
108	0.27414	154	4.004
110	0.31231	156	4.4393
112	0.35529	158	4.9171
114	0.40363	160	5.441

Table 2.2: Rb pressure versus temperature.

a scanning Fabry Perot (home-made, F.S.R = 1 GHz) for monitoring the laser mode. The laser must be single frequency and scan smoothly in the region of transition lines. The laser beam then passes through an acoustic-optic modulator. The zero-order is coupled into a fiber, and then goes to a home-made wavemeter with 1 GHz accuracy. The first order was focused into the center of the cell using a PCX lens (focal length=5cm) and retro-reflected by a concave dielectric mirror (R=10cm). The focusing points of the focused and that of the retro-reflected must be exactly the same to optimize the two-photon transition. This implies the retro-reflected beam must be the same as the incident beam anywhere. The adjustment of the position and angle of the retro-reflector mirror is sensitive to the signal strength. The reflected beam was directed back to the laser itself by adjusting the mirror. The laser feedback can

Decay routes	A value
$7S_{1/2} \rightarrow 6P_{3/2}$	$2.854 \times 10^6$
$7S_{1/2} \rightarrow 6P_{1/2}$	$1.409 \times 10^6$
$7S_{1/2} \rightarrow 5P_{3/2}$	$4.400 \times 10^6$
$7S_{1/2} \rightarrow 5P_{1/2}$	$2.640 \times 10^6$

Table 2.3: Decay channels of rubidium 7S state

be helpful as a signature of the perfect alignment.

The fluorescence is detected by a photomultiplier tube (PMT) and is demodulated using a lock-in amplifier (home-made). The demodulated signal and the transmission of the reference cavity are recorded by a computer using a data-acquisition (*DAQ*) card with a Labview program.

### 2.3.1 Laser system

The laser source is a commercial external-cavity diode laser (TOPTICA DL-100). The ECDL generates a power of 15 mW at 760 nm and a scanning range  $> 5$  GHz without mode hopping. The linewidth is estimated to be 1.5MHz by side of fringe method using a reference cavity.

### 2.3.2 Anamorphic prism pair

The beam profile of the ECDL output is approximately  $1 \times 3$  elliptical. Usually, this kind of beam profile is modified by minifying the major axis of the elliptical beam using anamorphic prism pair (APP) (see Fig. 2.4). APP minifies the beam size of one axis by a factor  $M$

$$M = \frac{\sqrt{1 - n^2 \sin^2 \Theta}}{\sqrt{1 - \sin^2 \Theta}} \quad (2.2)$$

Where  $n$  is the refractive index of the prism at the laser wavelength.

$\Theta$  is the angle of the prism. In this experiment,  $M=3$ .

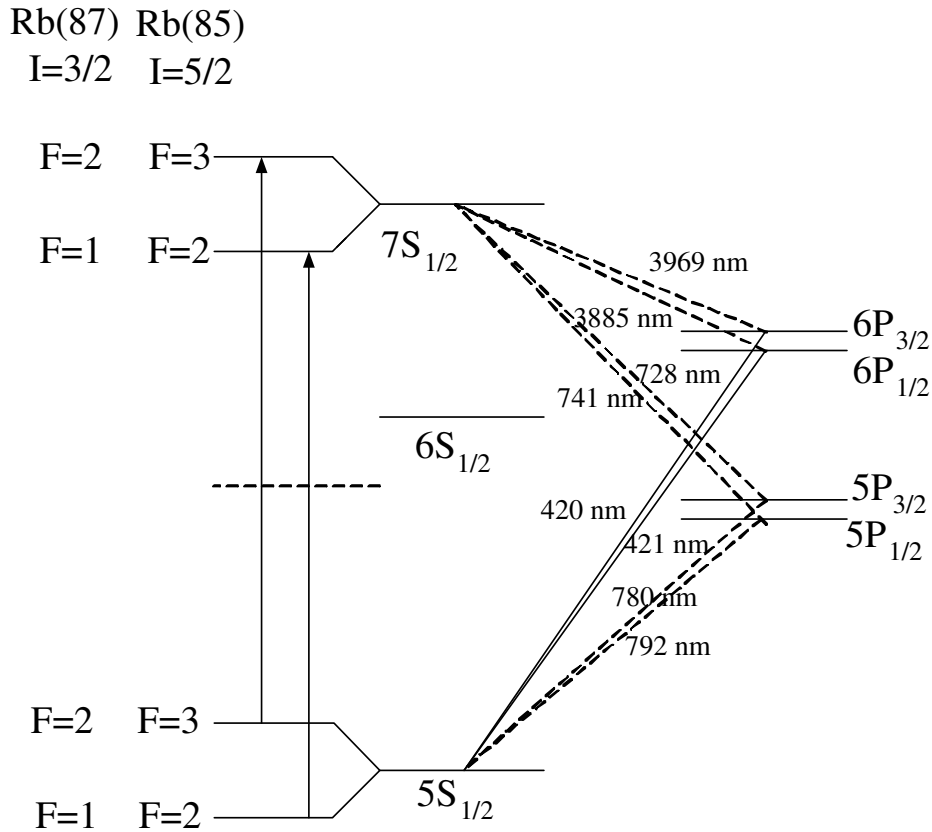


Figure 2.2: Partial energy level diagram of rubidium. (not scaled)

### 2.3.3 Cell and heating system

The rubidium cell has a length 25 mm and a diameter 25 mm (TOPTICA CE RB 25) and is contained in an aluminum box (see Fig. 2.5). The aluminum box is heated using three heating sheets. The cold finger of the cell sticks out of the box through an opening hole to keep its temperature  $20^\circ \sim 30^\circ\text{C}$  below the rest parts of the cell. The typical temperature of the cold finger is  $120^\circ\text{C}$  corresponding to a vapor pressure 0.5 mTorr and a number density  $5 \times 10^{21}$  atoms/m<sup>3</sup>.

### 2.3.4 Detecting system

Considering the quantum efficiency of the photomultiplier tube in different wavelengths, the 420 nm fluorescence is chosen for detection of the transition. A photomultiplier tube (HAMAMATSU R212) was used. The PMT is housed in a gray PVC

tube to reduce the background noise and providing a rigid mount (see Fig. 2.6). The fluorescence is filtered using a bandpass filter (Corion 450 FS80-25, center wavelength 450 nm, bandwidth 80 nm) to reduce the scattering light of the laser (760 nm).

### 2.3.5 light shielding system

The light shielding is a 400 mm $\times$ 130 mm $\times$ 250 mm box made from six ACETAL plates. The heating system, focusing lens and the concave mirror are inside this light shielding. The PMT tube sticks into the light shielding through opening a hole. The only one small aperture is opened for the incident laser light. Heating electricity and temperature probing are connected out through feed-through adapters.

## 2.4 Results

The four transition lines of rubidium  $5S \rightarrow 7S$  two-photon transition are all studied in this work. All transition lines are shown in Fig. 2.7. The hyperfine splittings of two isotopes are measured by the method of fringe interpolation. The result is 2754(4) MHz and 6202(4) MHz, for  $^{85}\text{Rb}$  and  $^{87}\text{Rb}$  respectively. This is in agreement with previous results, but less accurate. The isotope shift of  $5S \rightarrow 7S$  transition is 130(4) MHz. The measured linewidth is 3 MHz (see Fig. 2.8) that is larger than the natural linewidth, 899.5 kHz. The residual 2.1 MHz is contributed to the laser linewidth (1.5 MHz) and the transit time broadening (0.6 MHz). The laser beam is focused to a beam size of  $50\mu\text{m}$  ( $1/e^2$ ) in the cell by a PCX lens (focal length=5cm). Typically, the temperature of the cell is  $120^\circ\text{C}$ , corresponding to a thermal velocity of 340 m/s. The transit time of the moving atom inside the laser beam is  $0.147\mu\text{sec}$ , corresponding to a transit time broadening  $\sim 600$  kHz.

The transition linewidth is measured from  $140^\circ\text{C}$  to  $70^\circ\text{C}$ , and the linewidth remains the same under different temperature. This indicates pressure broadening does not dominate the broadening. The mean free path of rubidium atom at  $120^\circ\text{C}$  is  $\sim 3$  cm, which is significantly larger than the diameter of laser beam ( $\sim 50\mu\text{m}$ ). The pressure broadening is estimated as 50 kHz in 0.5 mTorr by extrapolating the experimental

data of the Rb-Rb collision in  $n > 10$  states [30]. There is no buffer gas in the rubidium cell.

The derivative-like error signal with  $\text{SNR} > 100$  is generated by frequency modulation technique (see Fig. 2.9). The laser frequency is modulated by modulating the injection current of the diode laser. This error signal is used to stabilize the laser frequency on the two-photon transition. Allan deviation is obtained by integrating the residual error signal with time (see fig. 2.10). Frequency stability is 7 kHz in 1 second integration time.

## 2.5 Reduction of laser linewidth

Vibration, electrical noise, and temperature variation cause the frequency and intensity noise of the diode laser. Since the spectral linewidth in our experiment is only a few MHz. It is important to have the laser with both long and short term stability for a low noise spectrum. In order to further stabilize the diode laser frequency, a tunable reference cavity is used.

The reference cavity is a confocal design, which has the advantage of easy alignment. The cavity consists of two mirrors ( $R=96\%$ ) and an Invar rod as spacer. One of the mirrors is glued on a cylindrical PZT tube for tuning the cavity length. A differential detector, which is capable of reducing the intensity noise caused by the fluctuation of the laser, is used to detect the transmission of the cavity. The diode laser is stabilized on the side fringe of the cavity to reduce its linewidth (see Fig. 2.12). The linewidth of the diode laser after stabilization is estimated to be 0.8 MHz by measuring the residual error signal.

## 2.6 Using light source doubled from 1520 nm ECDL by PPLN waveguide

The experimental setup is shown in Fig. 2.13. The  $5S \rightarrow 7S$  two-photon transition experiment was also performed using 1520 nm ECDL and PPLN waveguide. The laser

source is a commercial extended cavity diode laser (Anritsu MG9638A) with 6 mW output power between 1500 and 1580 nm and a scan range of 1.2 GHz. The 1520 nm laser beam from the ECDL was amplified to 95 mW using an EDFA (Technology Thesaurus Co). A fiber polarization controller rotated the laser polarization direction at the fiber output to be parallel to the extraordinary direction of the PPLN waveguide. The beam size was adjusted by use of an optical telescope, for optimal coupling into a 52-mm-long PPLN waveguide.

The PPLN waveguides used in the experiment were 52 mm long with 46 mm poling region. The poling period was 15  $\mu\text{m}$  with duty cycle of  $50\pm 5\%$ . This scheme generates a power of 10mW at 760 nm. The PPLN waveguide is housed in a Teflon case and covered by a glass plate. The housing is temperature controlled to be within  $0.1^\circ\text{C}$ . The 760 nm light was collimated from the PPLN waveguide by a half-sphere lens.

The result is as good as the previous results (760 nm ECDL experiment) (see Fig. 2.14 and Fig. 2.15). This indicates that the commercial 1520 nm diode laser can be directly locked on the two-photon transition by this frequency doubling scheme. The optical power of 760 nm radiation frequency doubled from 1520 nm ECDL is 10 mW, which is smaller than 760 nm ECDL (15 mW). The SNR of the signal is a little smaller than previous result due to less laser power in 760 nm.

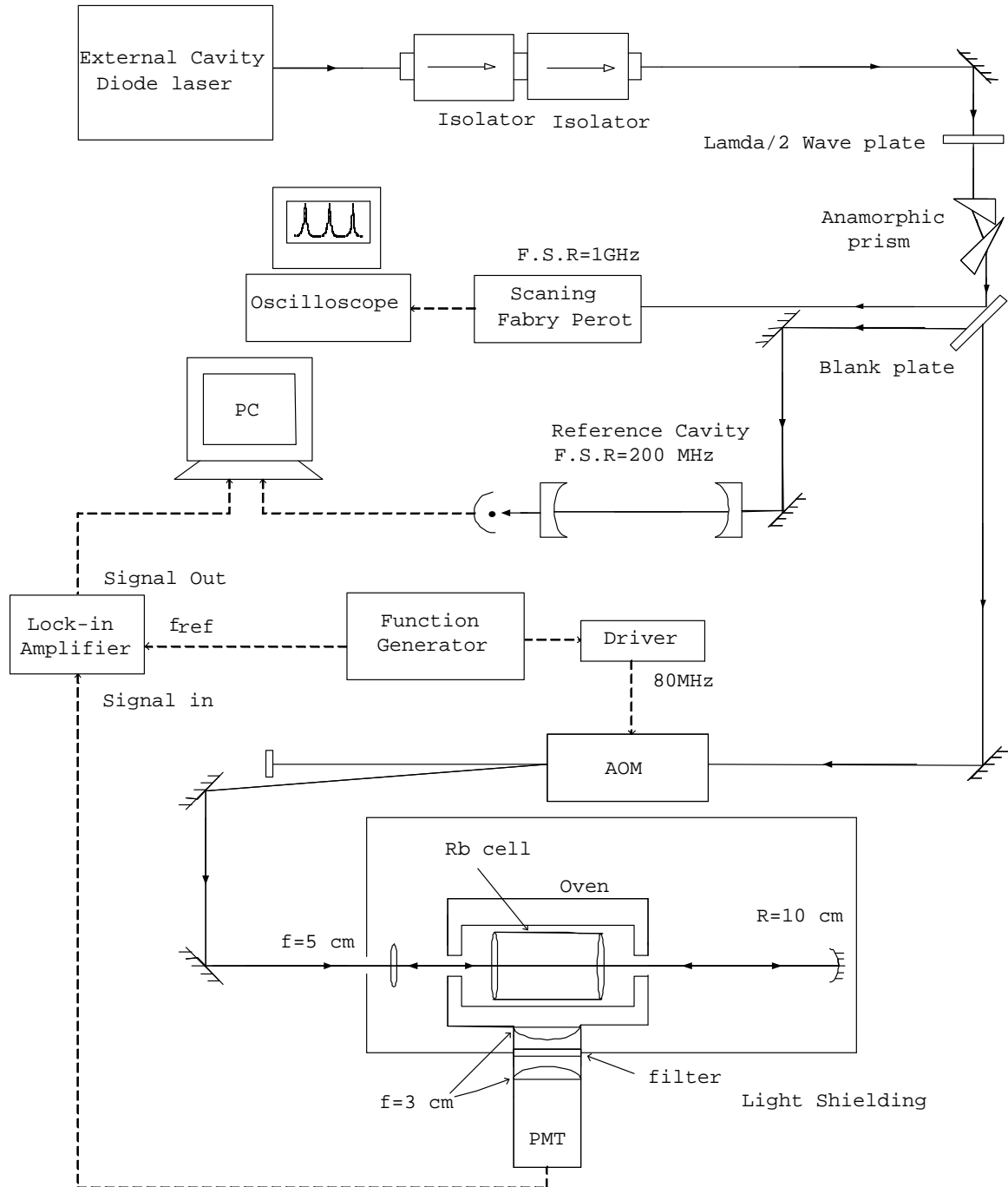


Figure 2.3: Experimental setup using 760 nm ECDL.

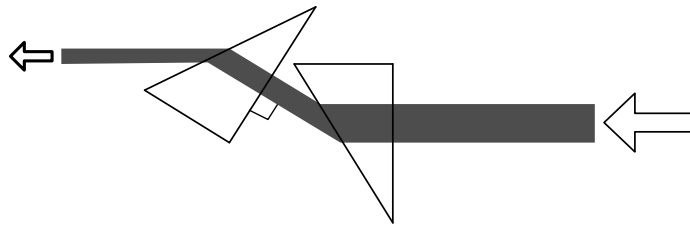
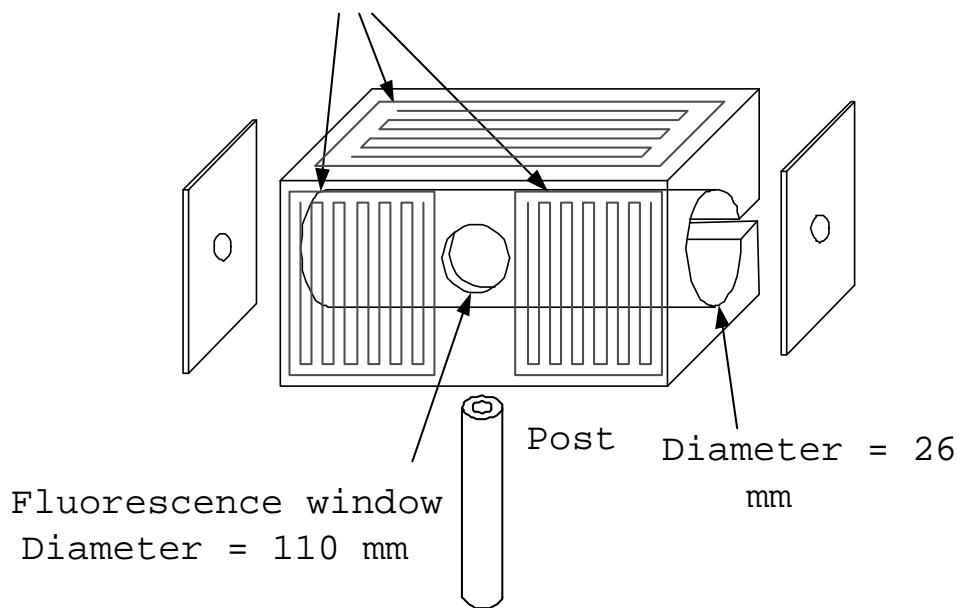
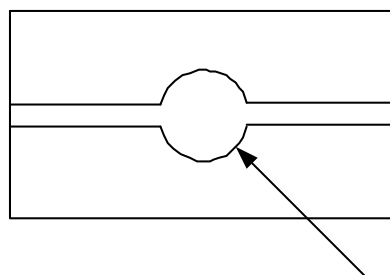


Figure 2.4: Anamorphic prism pair.

3 series connection heating sheets



(a) Front view



(b) End view

Figure 2.5: Heating cell design.

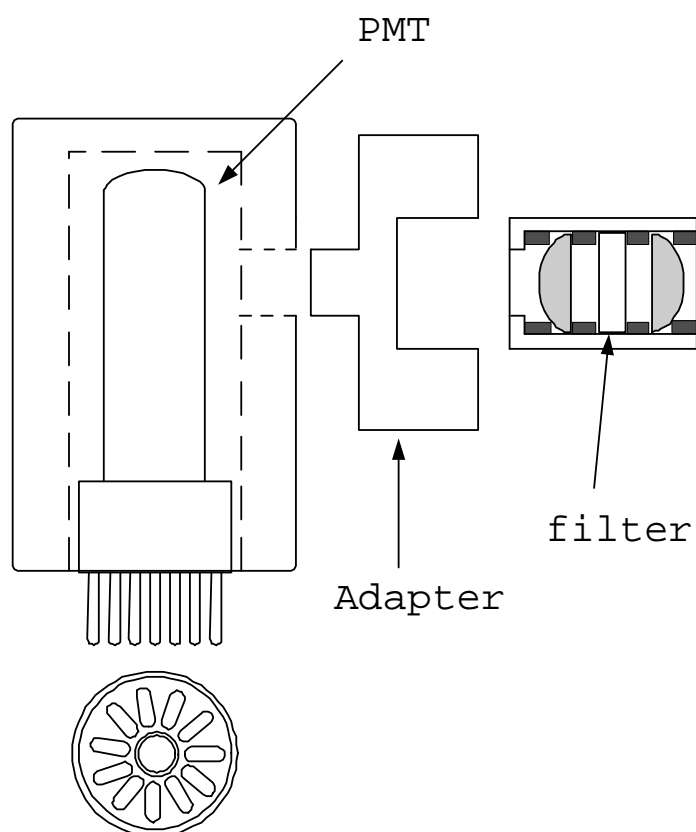


Figure 2.6: Fluorescence collection and detection system design.

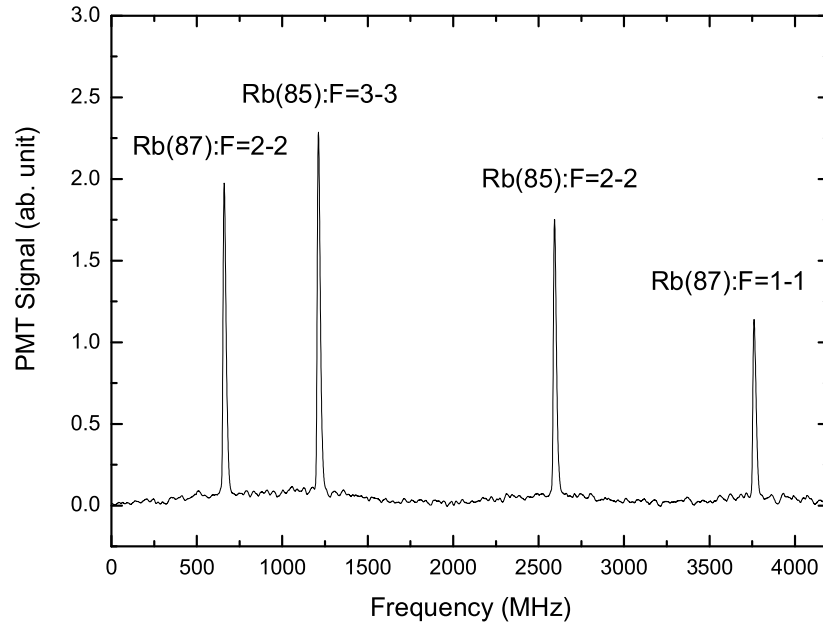


Figure 2.7: Spectrum of  $5S_{1/2} \rightarrow 7S_{1/2}$  two-photon transition. The frequency coordinate is determined by fringe marker of the reference cavity.

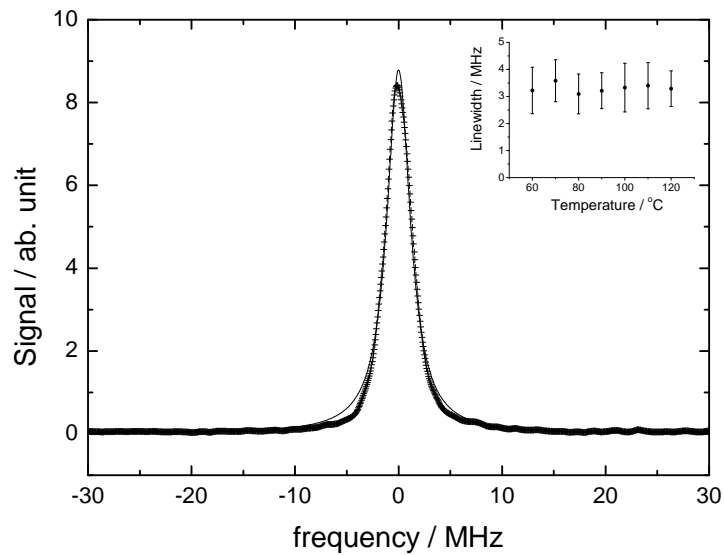


Figure 2.8: Lineshape of the  $^{85}\text{Rb}:5S_{1/2}(F=3) \rightarrow ^{85}\text{Rb}:7S_{1/2}(F=3)$  transition at  $110^\circ\text{C}$ . The signal is fitted to a Lorentzian lineshape with  $\text{FWHM}=2.8$  MHz and  $\text{SNR}=280$ . The inset shows the measured linewidth versus the temperature of vapor cell. Each point is the average of 10 measurements.

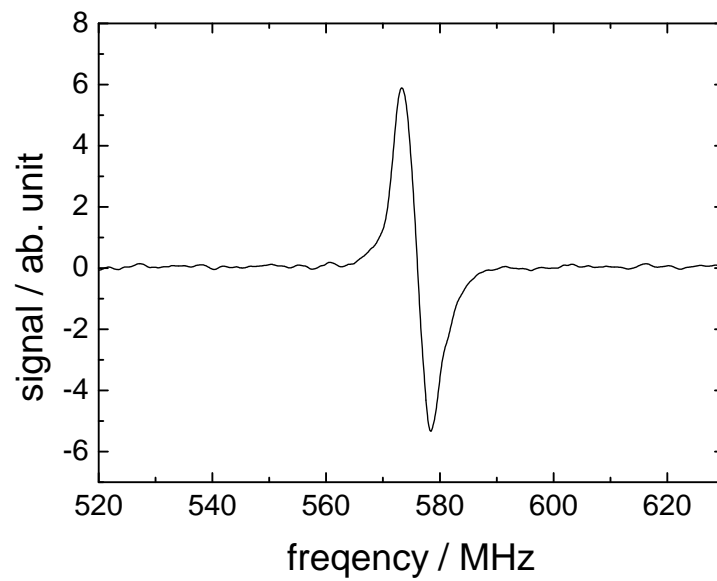


Figure 2.9: The zero-crossing lineshape generated by frequency-modulation spectroscopy. The SNR and linewidth (peak-to-peak) are 100 and 5.1 MHz, respectively.

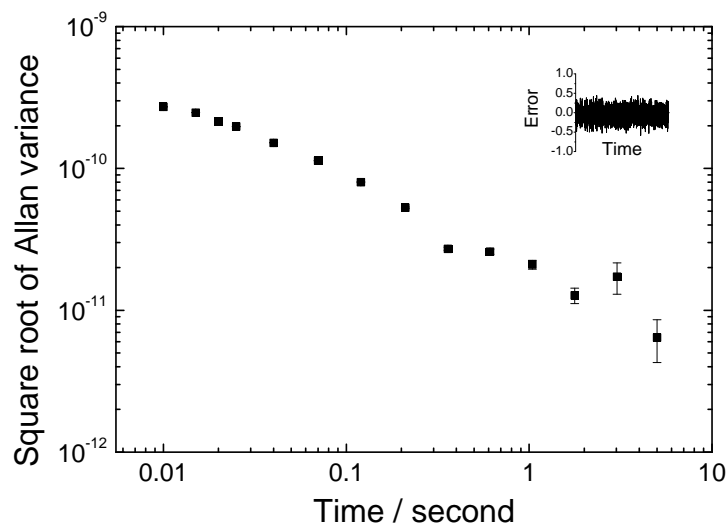


Figure 2.10: Allan deviation derived from the residual error signal while the laser was locked on the  $^{85}\text{Rb:F=3-3}$  two-photon transition. Inset shows the residual error signal.

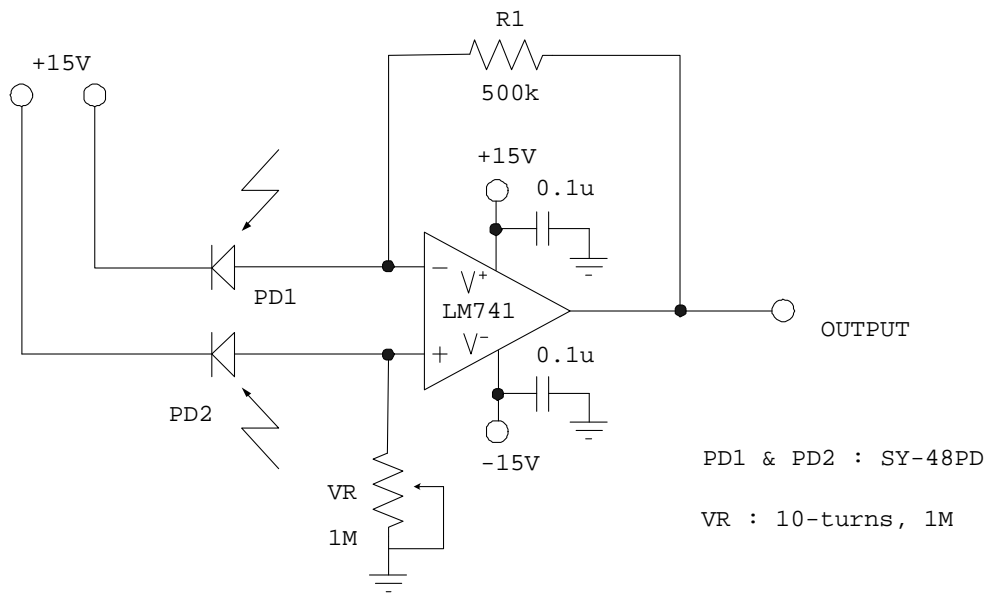


Figure 2.11: Differential detector.

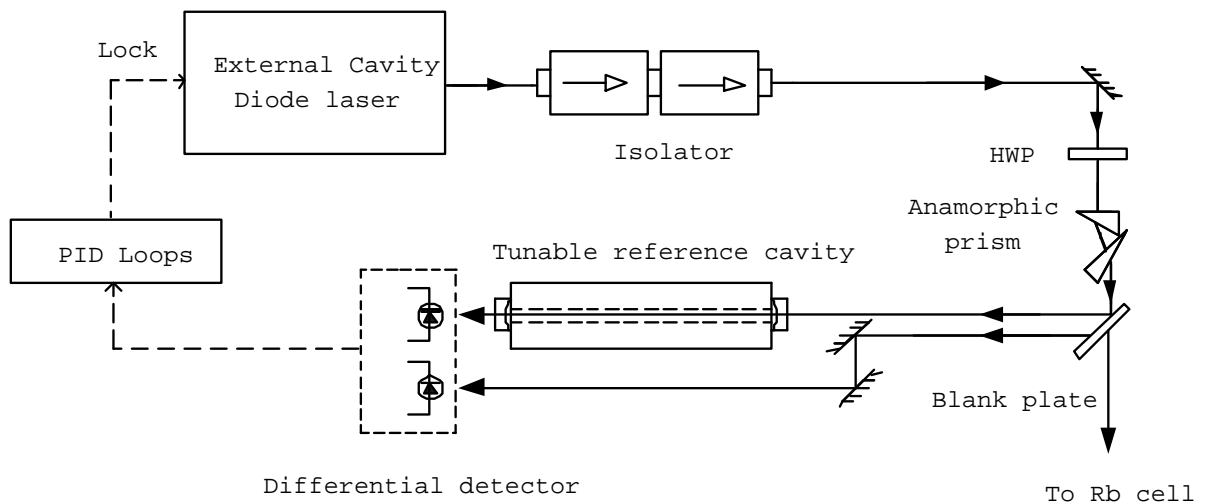


Figure 2.12: The ECDL is preliminary stabilized on the side fringe of a confocal tunable cavity. The linewidth of the diode laser after stabilization is 0.8 MHz.

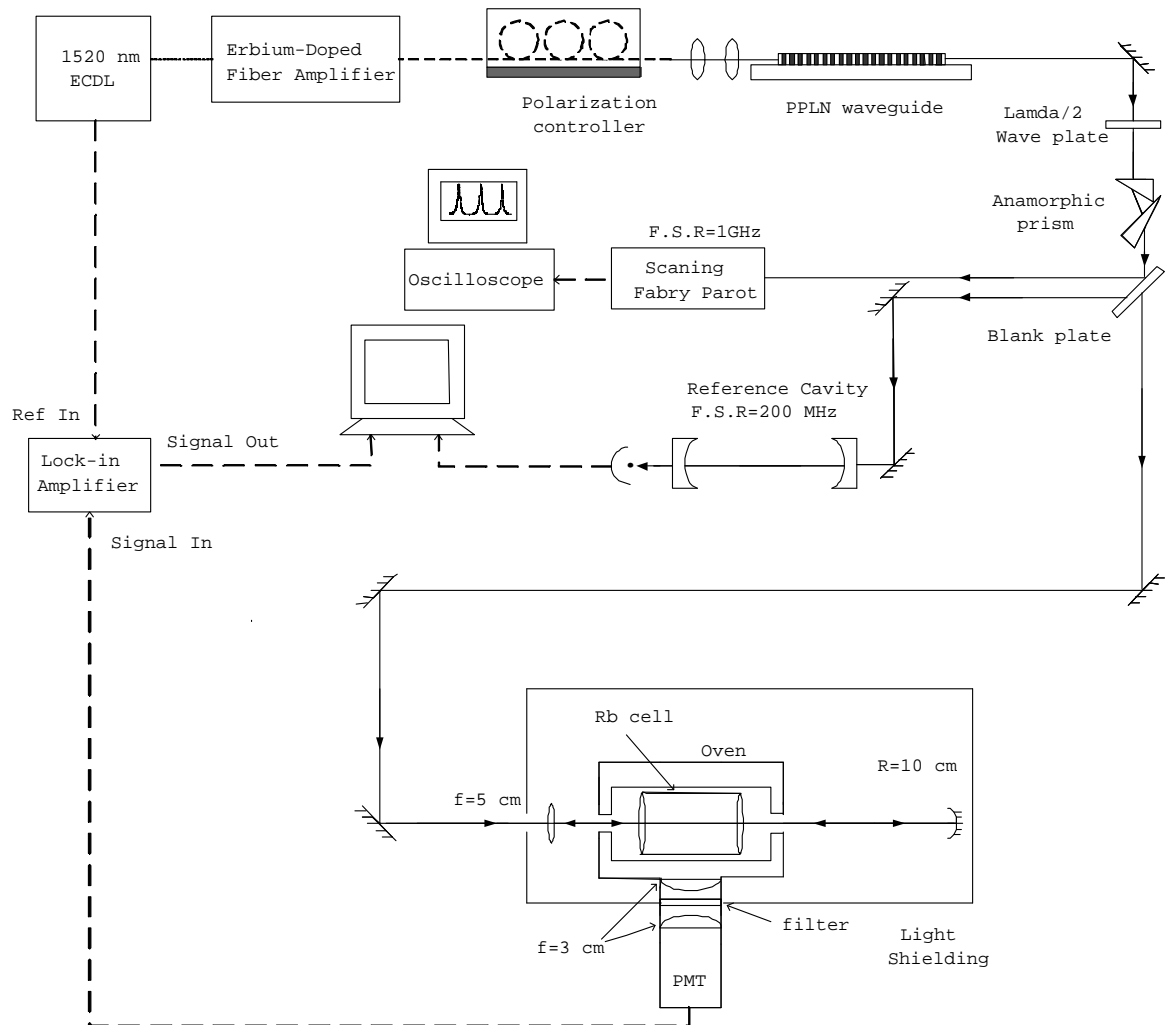


Figure 2.13: Experimental setup. The light source was frequency doubled from 1520 nm ECDL.

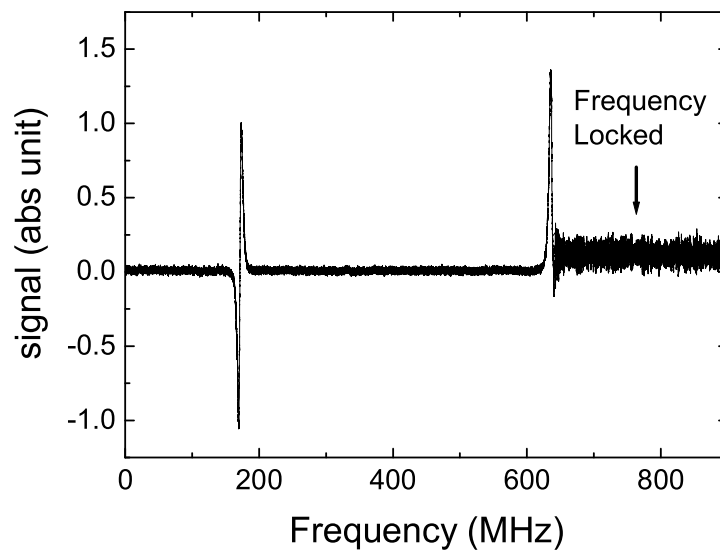


Figure 2.14: Derivative-like lineshape using frequency modulation technique. The signal-to-noise ratio is 30. The following noise shows the 1520 nm ECDL locked on  $^{85}\text{Rb:F=3-3}$  two-photon transition through frequency doubling.

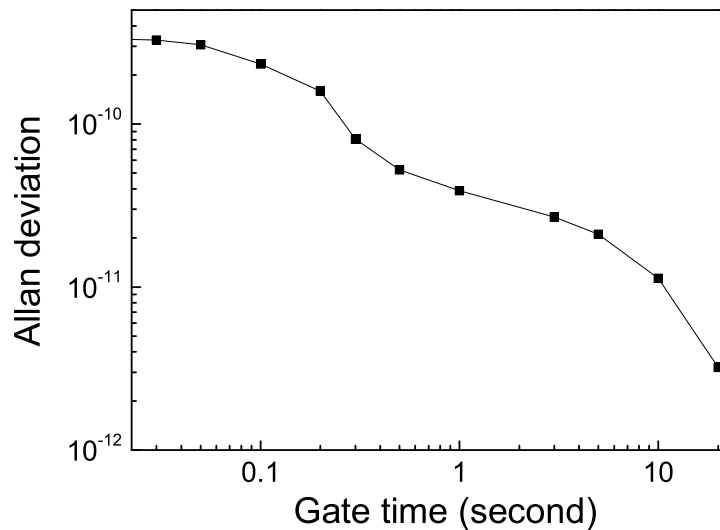


Figure 2.15: Allan deviation derived from the residual error signal while the 1520 nm ECDL was locked on  $^{85}\text{Rb:F=3-3}$  transition through frequency doubling.

# Chapter 3

## Absolute frequency measurement using optical femtosecond comb based on mode-locked Ti:sapphire laser

### 3.1 Femtosecond comb system

Femtosecond comb system in this experiment is setup by the Center for measurement Standards as shown in fig. 3.1. The femtosecond Ti: Sapphire laser has a repetition frequency of 1 GHz and pulse width of about 50 fs. It usually delivers an average power of more than 700 mW. A commercial photonic crystal fiber was used to expand the spectrum to contain octave. The PCF fiber has a core diameter of 1.8  $\mu\text{m}$  and has a zero dispersion wavelength at 710 nm. It generates a broad band frequency comb from 450-1100 nm with an average power of 200 mW.

The repetition frequency of the fs laser is phase-locked to a 1 GHz signal synthesized from a stable microwave source by controlling the cavity. The so-called f-2f technique is used to detect the offset frequency. Typical offset beat signal is 30 dB in a 100 kHz resolution bandwidth. The offset frequency is phase-locked to a synthesizer by

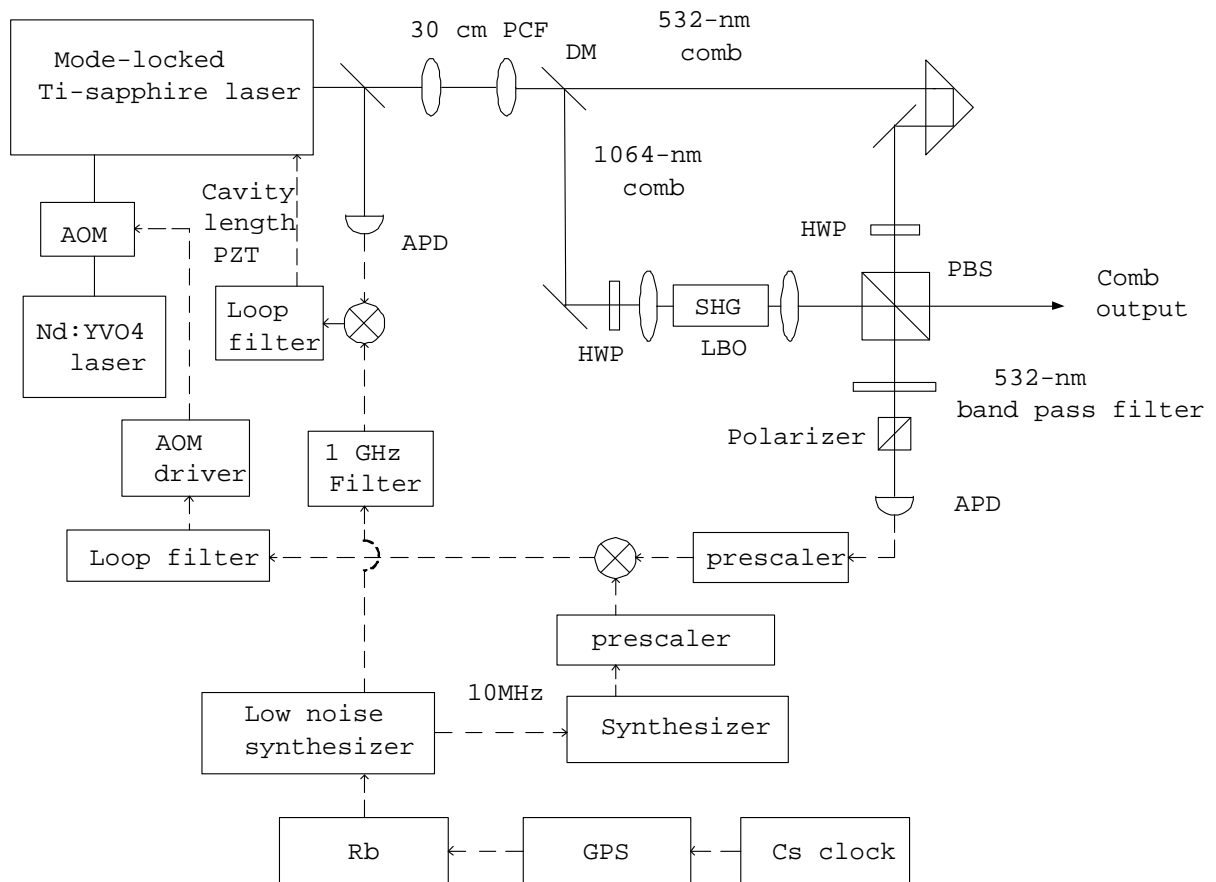


Figure 3.1: The femtosecond comb system setup by the Center for Measurement Standards. DMs: dichroic mirrors; APDs: avalanche photodiodes; SHG: second-harmonic generation; AOM: acoustic-optic modulator; PZT: piezoelectric transducer.

controlling the pump power with an acousto-optic modulator. The synthesizer is also referenced to the microwave source. The stable microwave source consists of a Rb clock and a low noise oven-controlled quartz oscillator for improving short term stability. The microwave source has a stability of better than  $2 \times 10^{-12}$  for integration time longer than 1 s. The frequency of the Rb clock is calibrated by a Global Positioning System (GPS) receiver. The uncertainty of the frequency calibration with one day of average is less than  $10^{-12}$ . The stabilized repetition frequency and offset frequency has residual peak-to-peak fluctuation of less than 2 mHz and 30 mHz, respectively. This contributes frequency fluctuations of less than 0.8 kHz to the frequency comb near 760 nm.

## 3.2 Method one: Stabilize the laser on the transition

The experimental setup of is shown in fig. 3.2. The laser source was doubled from 1520 nm ECDL using a PPLN waveguide. The laser frequency was locked on the two-photon transition by frequency modulation spectroscopy. Portions of stabilized

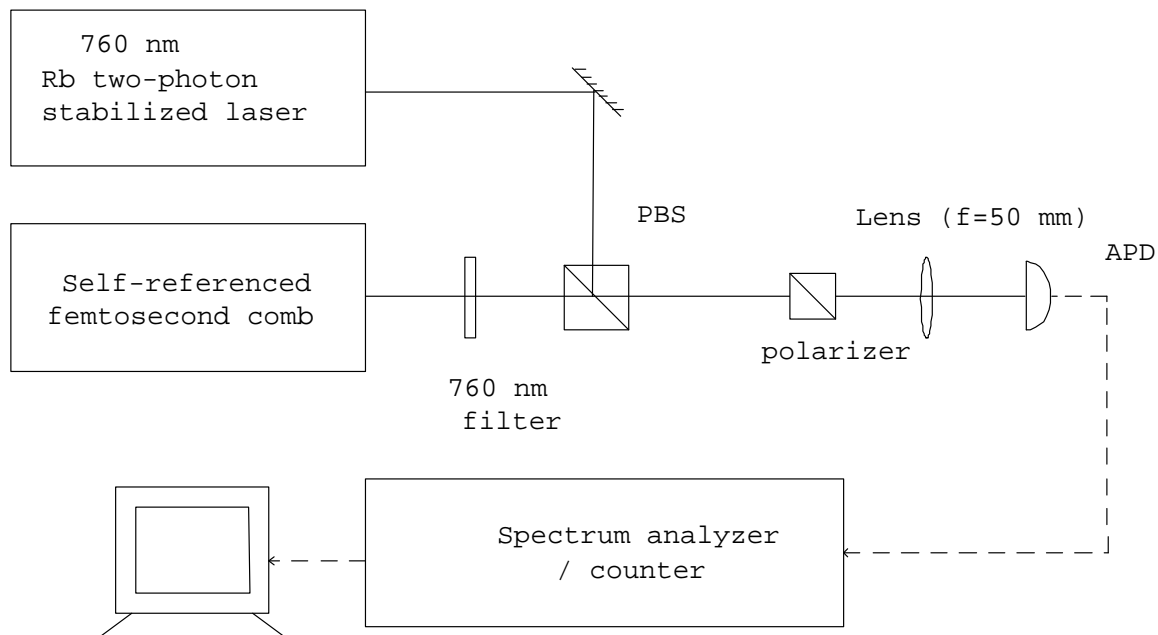


Figure 3.2: Absolute frequency measurement setup. The 760 nm laser is stabilized on the two-photon transition while the comb is self-referenced.

laser light ( $\sim 1\text{mW}$ ) and the self-referenced comb were combined together using a polarization beam splitter (PBS). A polarizer was used to project the polarization of the stabilized laser and comb on the same direction. An avalanche photo diode (APD) was used to detect the beat frequency between the stabilized laser and the comb spectrum. In order not to saturate the APD, the comb was filter by a 760 nm band pass filter (CVI, center wavelength=760 nm, bandwidth = 10 nm) to select comb lines near the stabilized laser. Besides a filter, we have tried a diffraction grating and an aperture to select comb lines near the stabilized laser. But the SNR is 5 dB smaller than using a filter.

A typical beat frequency spectrum is shown in fig. 3.3. The beat signal was amplified

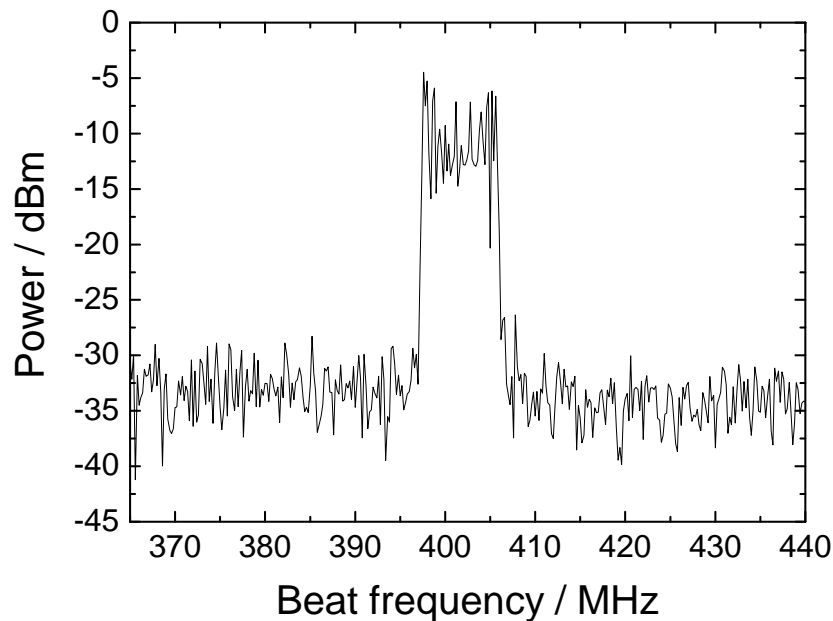


Figure 3.3: The beat signal between comb lines at 760 nm and the rubidium-stabilized laser. The resolution bandwidth is 100 kHz.

using two-stage pre-amplifier and a tunable bandpass filter (K&L) to select the beat note. The frequency of the beat note was counted using a counter (Agilent 53132 A). The counter is also referenced to the rubidium clock. In this experiment, the bandwidth of the beat note is about 6 MHz due to the frequency modulation of diode laser. Low frequency beat note is not suitable for counting because the bandwidth of the band pass filter (with constant Q factor) cannot accommodate the entire beat note signal. And this may result in counting error. This problem can be alleviated by counting the beat note in the 500~750 MHz region. The 1 GHz repetition rate signal is always too strong for us to count the beat note near 1GHz.

A typical beat frequency in counting is shown in Fig. 3.4. The Allan deviation of the beat frequency is  $\sim 3.5 \times 10^{-11}$  (14 kHz) at 1 second (see Fig. 3.5), which is only a little larger than that of previous result (see Fig. 2.15). This means the uncertainty of the beat frequency is dominated by the stability of 760 nm laser. The comb system contributes only 0.8 kHz.

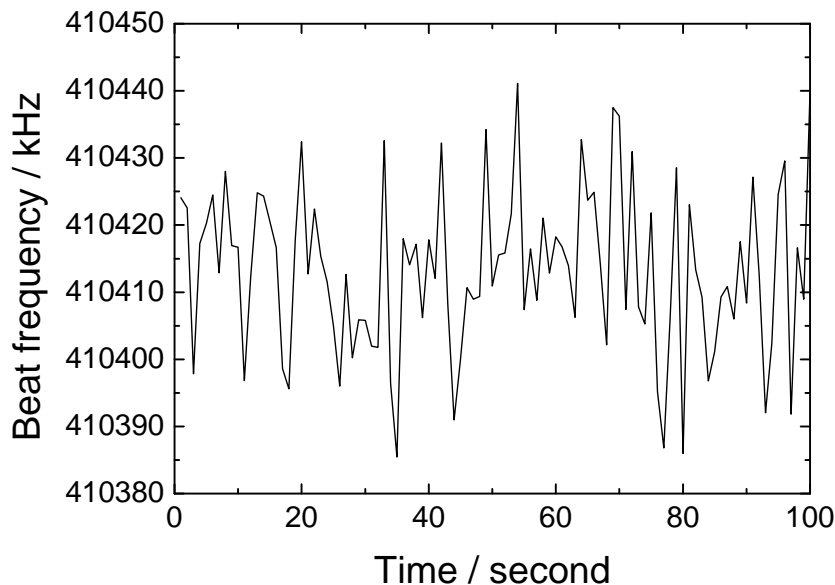


Figure 3.4: Beat frequency from counting the beat note. Gate time of the counter is 1 second. Typically, the standard deviation of the beat frequency is 15 kHz.

### 3.3 Method two: Offset-lock the laser on the comb

Another absolute frequency measurement scheme is that the laser was not stabilized on the two-photon transition but is offset-locked on the comb. The experimental setup is shown in fig. 3.6. The comb is self-referenced, and the laser is offset-locked on one of the comb lines. Therefore, the laser does not need frequency modulation. This eliminates the problem of the wide beat note bandwidth. This beat note is phase locked to a tunable synthesizer. Thus, the laser frequency is offset locked to one of the comb line by the frequency of the synthesizer. With tuning the frequency of the synthesizer, the laser can scan across the transition lines. The frequency of the synthesizer is controlled by a PC using GPIB interface. The 760 nm laser is chopped to provide the modulation and the signal of PMT is demodulated by a lock-in amplifier. This signal is simultaneously recorded while the synthesizer is scanning.

A typical signal is shown in fig. 3.7. By fitting the fluorescence signal, the difference between the center of transition and the self-referenced comb is known. This frequency is  $f_{beat}$  in eq.1.7. Together with the  $f_{rep}$  and  $f_o$ , the absolute frequency of the transition

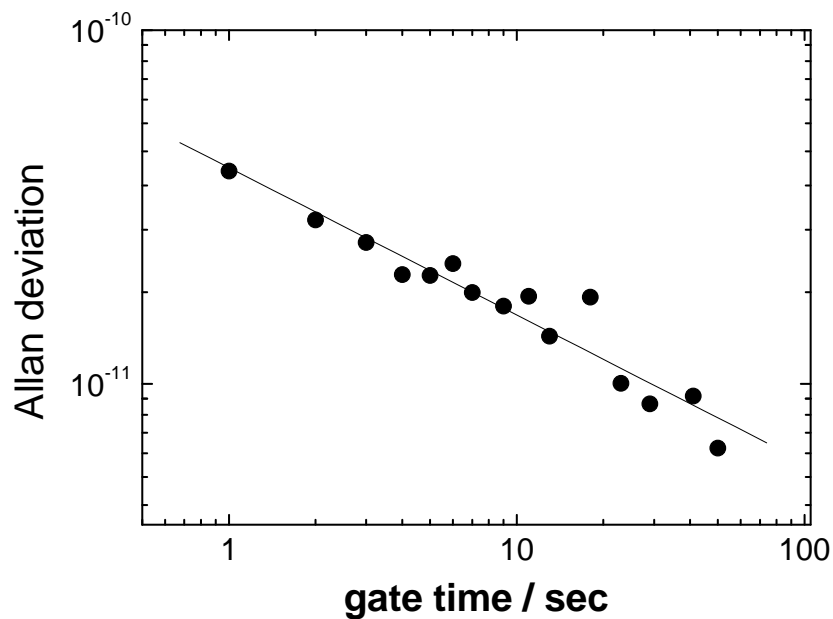


Figure 3.5: Allan deviation of the beat frequency between self-referenced comb and rubidium-stabilized laser.

can be calculated.

## 3.4 Results

### 3.4.1 Absolute frequencies of rubidium $5S_{1/2} \rightarrow 7S_{1/2}$ two-photon transitions

The absolute frequencies of the four hyperfine components in this two-photon transition are measured to an uncertainty of 20 kHz (see Table. 3.1). It is the first time that the frequency of this transition is measured. The four lines provide frequency standards in 760 / 1520 nm region.

### 3.4.2 Reproducibility of the measurements

The reproducibility of the measurement results is within 20 kHz in four measurements within 40 days (see fig. 3.8). Results of the two methods agree to each other.



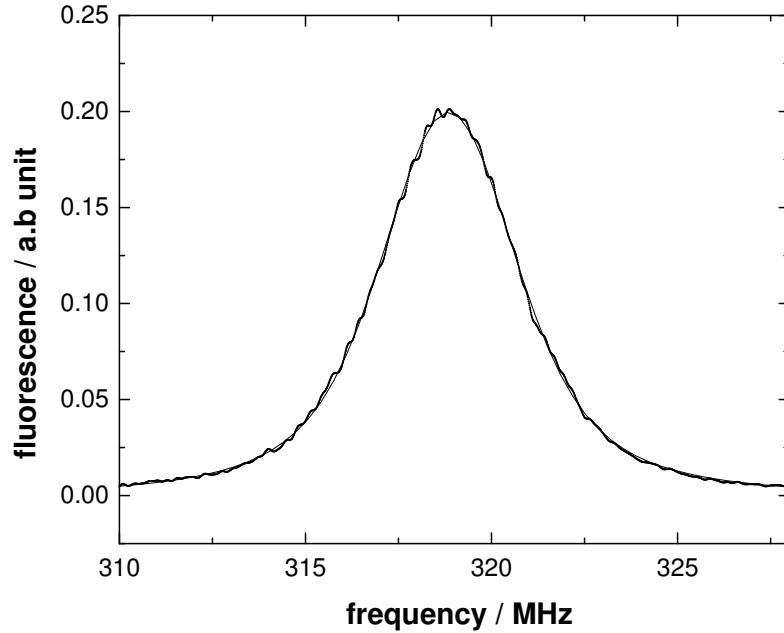


Figure 3.7: The signal of the transition using offset-lock scheme. The 760 nm laser is offset-locked on the comb line by the frequency of synthesizer. Frequency of the synthesizer is scanned using GPIB interface. Therefore, the laser frequency is scanned across the transition. The scanning range of synthesizer is 20 MHz in this measurement. Each scan is taken within 90 seconds.

The 760 nm laser source is frequency doubled from 1520 nm ECDL using PPLN waveguide. This scheme is capable of generating 10 mW 760 nm radiation. However, in order to have enough SNR ( $>20$ ), the 760 nm laser power must be larger than 4 mW. The tuning range of laser power is from 4 mW to 7 mW in the rubidium cell. Therefore, the line center difference between 4 mW and 7 mW laser power is less than 0.2 kHz, which is too small to be resolved in this measurement.

### Pressure shift

The pressure shift is estimated as -40 kHz/ mTorr by extrapolating the experimental data of the Rb-Rb collision in  $n > 10$  states [30]. Absolute frequencies are measured under different temperature (see Fig. 3.9). The measured pressure shift is -51.7(5.0) kHz / mTorr.

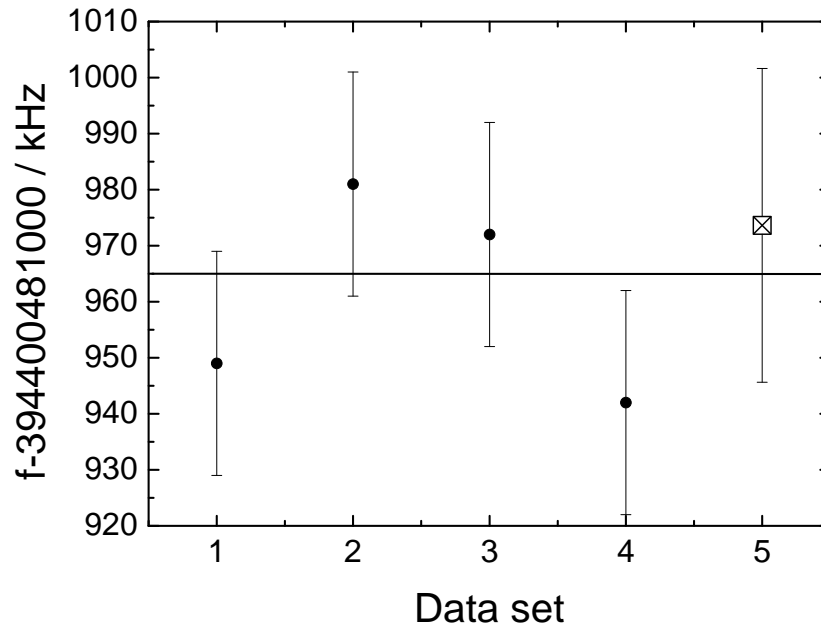


Figure 3.8: The measured frequency of the Rb<sup>87</sup> F=1-1 two-photon transition. The 760 nm laser power is 7 mW and the temperature of rubidium cell is 130°C. Data 1 ~ 4 are taken within 40 days using method 1 (stabilize the laser on the transition). Data 5 is taken using method 2 (offset-lock the laser on the comb line). Results of the two methods agree to each other.

### Second-order Doppler shift

Two-photon transition eliminates first-order Doppler shift, but not the second-order. The transition  $\nu_0$  is shifted by an amount  $-\nu_0 v^2/2c^2$ , where  $v$  is the speed of the atom [32]. For a temperature of 130°C, we obtain a shift of -240.6 Hz with respect to the 394 THz frequency.

### Blackbody radiation

The blackbody-radiation-induced dynamic Stark shifts of energy levels of hydrogen and different alkali atoms including rubidium at 300 K were calculated by Farley and Wing [33]. These calculations are extrapolated to a temperature of 130°C considering a  $T^4$  dependence. The shifts are -9 Hz for the  $5S_{1/2}$  level and -1340.5 Hz for the  $7S_{1/2}$  level. This leads to a shift of -665.8 Hz for the  $5S_{1/2} \rightarrow 7S_{1/2}$  two-photon transitions at

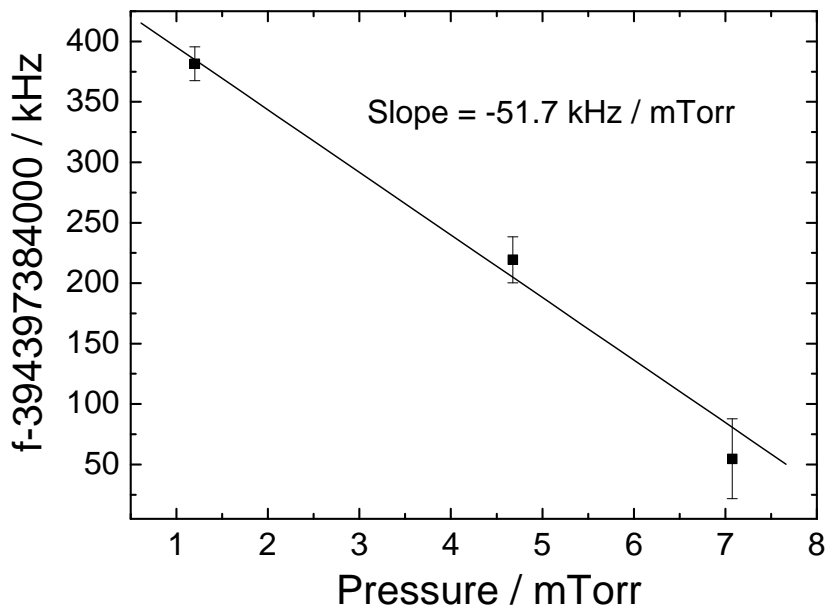


Figure 3.9: Frequency shift of the two-photon line center versus the pressure in rubidium cell. The 760 nm laser is stabilized on the  $\text{Rb}^{87}$  F=2-2 two-photon transition.

394 THz.

### Neighboring transitions

There are four lines in this transition (see Fig. 2.7). The lineshape distortion due to tails of neighboring transitions results in a frequency shift of the line center. These frequency shifts are evaluated by theoretically simulation of the lineshape.

The  $\text{Rb}^{87}$ :F=2-2 transition, which has the greatest shift due to neighboring transitions, is considered. The shift due to the Lorentzian profiles of the neighboring transitions is found to be +25 mHz, while the shift due to their Gaussian profiles amounts to be less than +1 mHz. The shift due to Doppler background of neighboring transitions is estimated to be +10 Hz.

### Electronic shifts

The offset at the output of the lock-in amplifier used to lock the laser frequency on the two-photon transition can influence the locked frequency. The derivative-like error

signal generated by FM spectroscopy has a slope of 500 Hz/mV (at 394 THz). The offset is assumed to have a maximum  $\pm 2$  mV corresponding to a frequency shift of  $\pm 500$  Hz at 394 THz.

### Summary

Table. 3.2 summarizes the values for different systematic shifts. After correction of these systematic effects, the absolute frequencies of rubidium  $5S_{1/2} \rightarrow 7S_{1/2}$  two-photon transition is shown in Table. 3.3.

Effect	Shift at 760 nm
Light shift	$-280 \pm 4$ Hz
Pressure shift	$-55.3 \pm 5.3$ kHz
Blackbody radiation	$-665.8 \pm 4$ Hz
Second-order Doppler shift	$-240.6 \pm 0.1$ Hz
Neighboring transitions	$< 10$ Hz
Electronics	$\pm 500$ Hz

Table 3.2: Summary.

Transition	Laser frequency (kHz)
Rb <sup>87</sup> F=2-2	394 397 384 439(20)(6)
Rb <sup>85</sup> F=3-3	394 397 906 983(20)(6)
Rb <sup>85</sup> F=2-2	394 399 282 821(20)(6)
Rb <sup>87</sup> F=1-1	394 400 482 021(20)(6)

Table 3.3: The absolute frequencies of rubidium  $5S_{1/2} \rightarrow 7S_{1/2}$  two-photon transition after correction of different systematic effects.

### 3.4.4 Hyperfine Constant of Rubidium 7S state

The hyperfine constant of the Rubidium 5S state has been measured to accuracy less than 1Hz [34], and from the absolute frequencies measured in this work, the upper level hyperfine constant can be obtained. The result is shown in Table. 3.4. Uncertainty of the hyperfine constant measured in this work is improved by a factor of 4, comparing with the previous best result.

To determine absolute frequency from eq.1.7, the  $n$  and the sign of the  $f_o$  and  $f_{beat}$

should be determined. Besides a wavemeter with sub GHz accuracy, hyperfine splitting can also be a judgement. If there are two hyperfine components in the measurement and their splitting has been measured to be within MHz accuracy, the frequency difference of the two absolute frequencies measured by comb should agree to the hyperfine splitting. This criterion selects the true  $n$  and the sign of the  $f_o$  and  $f_{beat}$ .

Isotope	this work	[35]	[34]
Rb <sup>87</sup>	319.759(28)	319.7(1)	318.1(32)
Rb <sup>85</sup>	94.658(19)	94.7(1)	94.00(64)

Table 3.4: The hyperfine constant A of rubidium 7S<sub>1/2</sub> state in MHz.

### 3.4.5 Isotope shift

The isotope shift of rubidium 5S<sub>1/2</sub>→7S<sub>1/2</sub> transition is deduced to be 131.567(73) MHz from this work. This result is in agreement with our previous result by fringe interpolation method, and is more precise [31].

# Chapter 4

## Conclusion

Absolute frequencies of rubidium  $5S_{1/2} \rightarrow 7S_{1/2}$  two-photon transition (760 nm) have been measured to an uncertainty of 20 kHz using optical femtosecond comb. This provides an optical frequency standard at 760 / 1520 nm region. Together with rubidium  $5S_{1/2} \rightarrow 5D_{1/2,3/2}$  two-photon transition (778 / 1556 nm), the rubidium cell can provide an accurate two-point calibration to cover the entire telecommunication band. The uncertainty of hyperfine constant in rubidium  $7S_{1/2}$  state is improved by a factor of four in this measurement, comparing with previous best result. And for the first time, isotope shift of this transition is measured to be 131.567(73) MHz. These fundamental constants are helpful in understanding the structure of the rubidium atom and testing fundamental theory.

By frequency doubling technique, a 1520 nm ECDL is stabilized on the two-photon transition. This provides a frequency standard in telecommunication band (1460-1530 nm, S-band).

In the future, possible improvements are summarized as following:

1. The transit time broadening can be reduced by increasing the laser beam size.
2. Enhanced cavity can be used to improve the SNR of the transition.

# References

- [1] J. C. Bergquist, *Symposium on Frequency Standards and Metrology*, 1st ed. (World Scientific, Singapore, 1995).
- [2] J. C. Berengut, V. A. Dzuba, and V. V. Flambaum, *Phys. Rev. A* **68**, 022502 (2003).
- [3] L. P *et al.*, *Eur. Phys. J. D.* **3**, 201 (1998).
- [4] H. Schnatz *et al.*, *Phys. Rev. Lett.* **76**, 18 (1996).
- [5] A. Arie and R. L. Byer, *J. Opt. Soc. Am. B* **11**, 866 (1994).
- [6] D. A. Tyurikov, M. A. Gubin, A. S. Shelkovnikov, and E. V. Kovalchuk, *IEEE Trans. Instrum. Meas.* **44**, 166 (1995).
- [7] K. Nakagawa, M. de Labachellerie, Y. Awaji, and M. Kourogi, *J. Opt. Soc. Am. B* **13**, 2708 (1996).
- [8] Y. Millerioux *et al.*, *Opt. Comm.* **108**, 91 (1994).
- [9] G. Scoles, D. Bassi, U. Buck, and D. Lainé, *Atomic and Molecular Beam Methods*, 1st ed. (Oxford University Press, New York, 1998).
- [10] M. J. Snadden, A. S. Bell, R. B. M. Clarke, and E. Riis, *J. Opt. Soc. Am. B* **14**, 544 (1997).
- [11] S. Chu and C. H. Townes, *Biographical Memoirs.* **83**, (2003).
- [12] L. Hilico *et al.*, *Eur. Phys. J. AP.* **4**, 219 (1998).
- [13] T. Andreae *et al.*, *Phys. Rev. Lett.* **69**, 1923 (1992).
- [14] G. Grynberg and B. Cagnac, *Rep. Prog. Phys.* **40**, 791 (1977).
- [15] B. W. Shore and D. H. Menzel, in *Principles of Atomic Spectra* (John Wiley and Sons, New York, 1969), p. 33.
- [16] B. W. Shore and D. H. Menzel, in *Principles of Atomic Spectra* (John Wiley and Sons, New York, 1969), p. 71.
- [17] G. Hagel *et al.*, *Opt. Comm.* **160**, 1 (1999).

- 
- [18] M. Niering *et al.*, Phys. Rev. Lett. **84**, 5496 (2000).
- [19] F. Nez, F. Biraben, R. Felder, and Y. Millerioux, Opt. Comm. **102**, 432 (1993).
- [20] S. T. Cundiff, J. Ye, and J. L. Hall, Rev. Sci. Instrum. **72**, 3749 (2001).
- [21] B. I. des Poids et Mesures (BIPM), *Report of the 86th meeting of the Comité International des Poids et Mesures (CIPM)*, (Paris 1997).
- [22] M. Poulin, C. Latrasse, D. Touahri, and M. Tetu, Opt. Comm. **207**, 233 (2002).
- [23] D. Touahri *et al.*, Opt. Comm. **133**, 471 (1997).
- [24] P. Otto *et al.*, J. Chem. Phys **282**, 289 (2002).
- [25] R. E. Honig, RCA Rev. 567 (1962).
- [26] B. R. Bulos, R. Gupta, and W. Happer, J. Opt. Soc. Am. **66**, 426 (1976).
- [27] R. Gupta, W. Happer, L. K. Lam, and S. Svanberg, Phys. Rev. A **8**, 2792 (1973).
- [28] A. Rose and I. Lindgren, Physica Scripta. **6**, 109 (1972).
- [29] R. E. Ryan, L. A. Westling, and H. J. Metcalf, J. Opt. Soc. Am. B **10**, 1643 (1993).
- [30] B. P. Stoicheff and E. Weinberger, Phys. Rev. Lett. **44**, 733 (1980).
- [31] M. S. Ko and Y. W. Liu, Opt. Lett. **29**, (2004).
- [32] B. Cagnac, G. Grynberg, and F. Biraben, Le J. Phys. **34**, 845 (1973).
- [33] J. W. Farley and W. H. Wing, Phys. Rev. A **23**, 2397 (1981).
- [34] E. Arimondo, M. Inguscio, and P. Violino, Rev. Mod. Phys. **49**, 31 (1977).
- [35] M. J. Snadden, A. S. Bell, E. Riis, and A. I. Ferguson, Opt. Comm. **125**, 70 (1996).